University of Louisville

ThinkIR: The University of Louisville's Institutional Repository

Electronic Theses and Dissertations

5-2013

Mechanical characterization of MEMS bi-stable buckled diaphragms.

Isaac James Phelps
University of Louisville

Follow this and additional works at: https://ir.library.louisville.edu/etd

Recommended Citation

Phelps, Isaac James, "Mechanical characterization of MEMS bi-stable buckled diaphragms." (2013). *Electronic Theses and Dissertations.* Paper 1129.
https://doi.org/10.18297/etd/1129

This Master's Thesis is brought to you for free and open access by ThinkIR: The University of Louisville's Institutional Repository. It has been accepted for inclusion in Electronic Theses and Dissertations by an authorized administrator of ThinkIR: The University of Louisville's Institutional Repository. This title appears here courtesy of the author, who has retained all other copyrights. For more information, please contact thinkir@louisville.edu.

MECHANICAL CHARACTERIZATION OF MEMS BI-STABLE BUCKLED DIAPHRAGMS

By

Isaac James Phelps
B.S., University of Louisville, 2012

A Thesis
Submitted to the Faculty of the
University of Louisville
J. B. Speed School of Engineering
as Partial Fulfillment of the Requirements
for the Professional Degree

MASTER OF ENGINEERING

Department of Mechanical Engineering

May 2013

MECHANICAL CHARACTERIZATION OF
MEMS BI-STABLE BUCKLED DIAPHRAGMS

Submitted by:___________________________________
Isaac James Phelps

A Thesis Approved On

____
(Date)

by the Following Reading and Examination Committee:

____
Dr. Thomas Berfield, Thesis Director

____
Dr. Roger Bradshaw

____
Dr. Palaniappan Sethu

ACKNOWLEDGEMENTS

I would like to thank Dr. Berfield, my thesis advisor, whose continued guidance and support made this project possible. I would also like to thank Daniel Porter, who did much of the device fabrication and LabView program writing. Additionally, I would like to thank my committee members, Dr. Bradshaw and Dr. Sethu. I would like to thank the Department of Mechanical engineering and the University of Louisville. Finally, I would like to thank my family for all of their support over the course of all my education.

ABSTRACT

Bi-stable buckled MEMS (micro-electromechanical systems) diaphragms have a myriad of uses in the MEMS field for their large out-of-plane deflections. Buckling is a phenomenon brought upon by a compressive stress. Diaphragms are large aspect ratio, circular structures similar to membranes, where the thickness of the diaphragm is much smaller than its diameter. Diaphragms differ from membranes by the amount of bending stiffness. Membranes have negligible bending stiffness and are a common structure analyzed in mechanics of materials, whereas diaphragms have much larger stiffness.

Diaphragms were created in the cleanroom by thermally growing silicon dioxide on a silicon wafer. A structural polyimide layer was added on top of the silicon dioxide. The created diaphragms demonstrate bi-stability, meaning that they can be switched either up or down using an applied pressure. After the pressure is removed the diaphragms remain in their new respective states. The pressure required to switch the membranes is known as the actuation or snap-through pressure, and is of primary interest. The vertical displacement of the center of the diaphragms, known as the buckled height, is also of interest. A finite element model of the diaphragm was created using ANSYS. This model was used to generate both actuation pressure and buckled height data. These two data sources are compared extensively in an attempt to further understand the behavior of the experimental system.

Buckled height data between experimental data and the finite element model were found to match well. This information can be used in the production of micro-valves and micro-actuators in the future. Actuation pressure found from the finite element model follows the trend and closely models the values of experimental data for a range of

membranes. Other effects not accounted for in the finite element model probably contribute to the difference between the two.

TABLE OF CONTENTS

	Page
APPROVAL PAGE	ii
ACKNOWLEDGEMENTS	iii
ABSTRACT	iv
LIST OF TABLES	vii
LIST OF FIGURES	viii
I. INTRODUCTION	1
A. Background and Motivation	2
II. PROCEDURE	
A. Fabrication	14
B. Pressure Testing	16
C. ANSYS Simulation	22
III. RESULTS	
A. Experimental Pressure Testing Results	28
B. ANSYS Modeling Results	36
IV. DISCUSSION	44
V. CONCLUSIONS	53
VI. FUTURE WORK	54
VII. REFERENCES	57
VIII. APPENDIX I	59
IX. APPENDIX II	63

LIST OF TABLES

Page

Table 1. Description of tested dies 29

Table 2. Standard deviation of dies b, c, and d used in experimental testing. 36

Table 3. Buckled Heights of Die E 43

LIST OF FIGURES

Page

Figure 1. Assumed shape function from Timoshenko with variables noted...................... 3

Figure 2. Deflection curves for 900μm (a) and 300μm (b) diameter diaphragms [8]. 3

Figure 3. Vertical deflection curve of 900μm diameter membrane................................. 4

Figure 4. Cross-section illustration of a square, buckled diaphragm [12]........................ 6

Figure 5. Buckled square diaphragms of different dimensions 7

Figure 6. Finite element simulation of the buckled profile along the diagonal 9

Figure 7. Comparison between analytical and finite element model of Ayela *et al* [13]. 10

Figure 8. Silicon diaphragm thickness versus calculated deflection of the diaphragm... 11

Figure 9: Comparison of analytical and finite element data [13]. 12

Figure 10: 300μm diameter diaphragm from Gowrishetty et al. [14]............................ 13

Figure 11. L-Edit mask layout for the 100mm diameter wafer. 15

Figure 12. Array mounted in old test fixture with pressure sensor connected. 16

Figure 13. Test process schematic. 17

Figure 14. Wheatstone bridge and National Instruments module.................................. 18

Figure 15. Consecutive images showing 700μm diameter diaphragm 19

Figure 16. New test fixture solid model... 20

Figure 17. Bottom section of the new test fixture... 20

Figure 18. New test fixture with component callouts 21

Figure 19. Element plot showing boundary conditions at right end.............................. 22

Figure 20. Element plot of axisymmetric shell model.. 23

Figure 21. Quarter symmetry expansion of Axisymmetric Shell209 model 24

Figure 22. Element plot showing boundary conditions for thermal analysis of stress. 26

Figure 23. Stress versus temperature plot of ANSYS Plane 183 simulation................... 26

Figure 24. Representative ANSYS simulation loading plot... 27

Figure 25. Released dies after manufacture – array 1 highlighted. 28

Figure 26. Graphical representation of switching modes. 30

Figure 27. Backside of array 1 showing loss of smallest diaphragms (highlighted). 31

Figure 28. Topside of array 1, smallest diaphragms are not visible. 31

Figure 29. Array 1 experimental switching pressures 33

Figure 30. Array A experimental switching pressures.. 33

Figure 31. Experimental data from Dies B, C and D.. 34

Figure 32. Complete actuation data for a 500um diameter diaphragm from array 1........ 35

Figure 33. Buckling analysis illustrating inherent instability of a 1500μm diameter...... 37

Figure 34. Successful actuation of diaphragm, 400 diameter.. 38

Figure 35. ANSYS FEA data and Array A experimental data. 39

Figure 36. Experimental and ANSYS switching down data for tested dies and arrays... 40

Figure 37. ANSYS and experimental switching up data for tested dies and arrays.. 41

Figure 38. Die E experimental and ANSYS switching data... 41

Figure 39. Buckled height comparison between ANSYS and experimental data. 42

Figure 40. Delamination illustration for up and down switching modes......................... 44

Figure 41. Image of diaphragm showing boundary conditions (highlighted). 45

Figure 42. SEM image of a sidewall showing silicon "grass" (highlighted). 46

Figure 43. Diaphragm section showing silicon micro-columns or "grass"...................... 47

Figure 44. Illustration of undercutting and its effect on switching................................. 48

Figure 45. Cross-section of a diaphragm showing effects of DRIE 48

Figure 46. DRIE trench radius, Chen *et al*. [17]. 49

Figure 47. Die E, 1500µm diaphragm, non-eigenvalue buckling down. 50

Figure 48. Element plot in ANSYS of new model showing element type 55

Figure 49. Eigenvalue buckling analysis showing shell and plane elements. 55

Figure 50. Speckled image from die E. 56

I. INTRODUCTION

Micro-electro-mechanical systems (MEMS) are devices with dimensional length scales on the order of a micron, or one-millionth of a meter. In many MEMS sensor devices, electrical transducers are often used to relate minute, but measureable deformations induced within MEMS structures by some external phenomena (acceleration, force, pressure, etc.). These devices can be used for a multitude of applications, including zero-power pressure sensors [1], large displacement actuators [2], BIO-MEMS to measure pressures within a human body [3]. Remote pressure sensors that can be read using light, such as a Bragg grating, allowing for many more applications in harsher environments [4-6]. Diaphragms that operate in a large deflection regime, involving the stability of buckled structures, offer many potential performance benefits, but also present greater challenges in prediction of behavior. A fundamental understanding of the mechanical behavior of the diaphragms, especially the influence of fabrication parameters on the experimental repeatability, is critical for designing these structures for practical MEMS applications.

The work presented herein, focuses on micro-scale diaphragms composed of a combination of silicon dioxide (SiO_2) and polyimide, supported and constrained by a bulk silicon substrate. With this material system, compressive stresses naturally develop in the oxide layer during the wafer oxidation procedure. If the magnitude of the residual compressive stress is large enough, the diaphragm can enter a buckle mode upon release from the substrate constraint (depending on the diaphragm dimensions). MEMS scale diaphragms fabricated in the cleanroom are experimentally tested under pressurization, and compared to ANSYS models simulating diaphragm behavior. The deviations in

mechanical behavior of the model and experimentally tested diaphragms are discussed and correlated with experimental observations.

A. Background & Motivation

To facilitate pressure monitoring, many applications make use of a diaphragm that separates a reference pressure from the applied pressure being measured. The pressure differential across the diaphragm induces deformation of the structure, the magnitude of which can then be related to the pressure loading given that the material properties are known. Thus, accuracy in predicting the pressure-deflection relationship and a thorough understanding of the mechanical behavior of diaphragm structures is critical for the design of these systems. First, a brief review is presented of some simple diaphragm geometries that have been analyzed previously by others. Part of the motivation of this work is to help identify sources of deviations between diaphragm mechanical behavior predicted by theory and simulations and the actual behavior found experimentally.

Timoshenko worked extensively with the theory of plates in shells in the early 20th century. His work is the basis for much of the current understanding of the behavior of membranes and diaphragms. Theoretical modeling of a thin plate depends upon the assumption of a shape function. The plate is assumed to be symmetric and clamped or fixed at the wall. The plate is also assumed to be homogeneous. All further mathematical modeling stems from these assumptions. The symmetric shape function is

$$w = w_0 \left(1 - \frac{r^2}{a^2}\right)^2 \qquad (1)$$

where w is the height out of plane; w_0 is the initial height of the center of the diaphragm in a un-loaded, buckled state; r is the radial location from the center of the plate; and a is the total radius of the plate [7]. These variables are shown graphically in Figure 1.

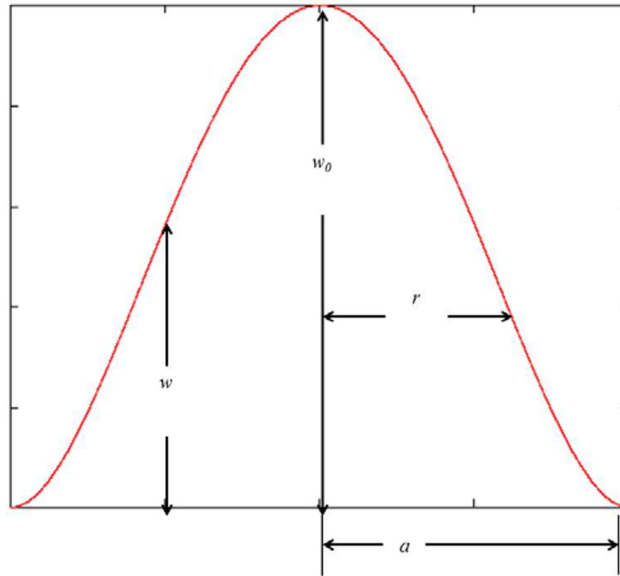

Figure 1. Assumed shape function from Timoshenko with variables noted.

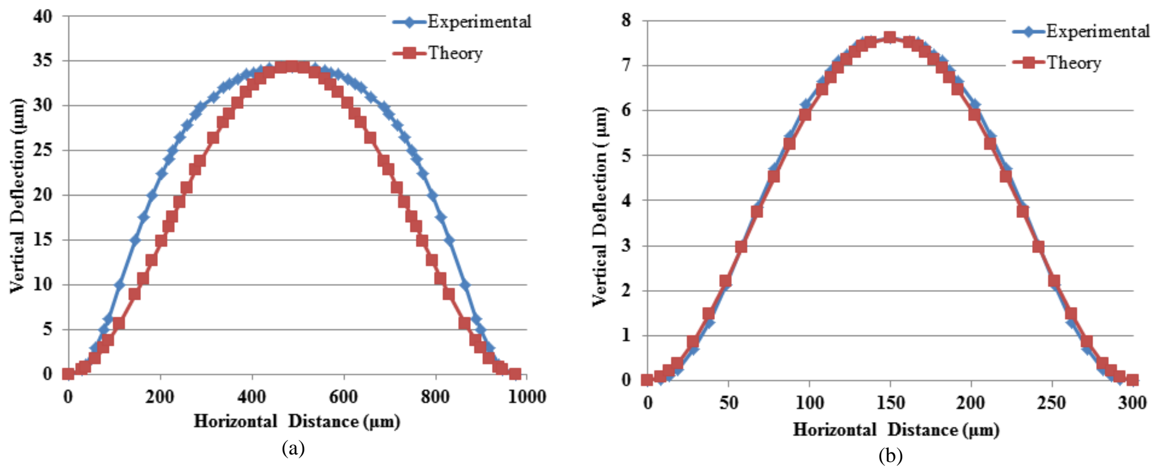

Figure 2. Deflection curves for 900µm (a) and 300µm (b) diameter diaphragms [8].

Equation (1) is then used to approximate the bending energy and the strain energy of the diaphragm. Timoshenko showed that as w_0 increases the deflection is no longer proportional to the load applied and the rigidity of the plate increases with deflection. The vertical deflections of the 300μm and 900μm diaphragms shown in Figure 2 are plotted against the theoretical shape function given by equation (1). The theoretical model clearly matches well with the smaller diameter diaphragm. However, the larger diameter does not match as well, except for the boundary and center of the membrane. As pressure is applied to a larger membrane, a dimple can form, as in Figure 3. The dimple forms prior to the actuation pressure being reached. This dimple affects the potential energy stored within the membrane. The changes to the potential energy are not modeled in theory. This irregular behavior is frequently modeled using finite element analysis packages [7].

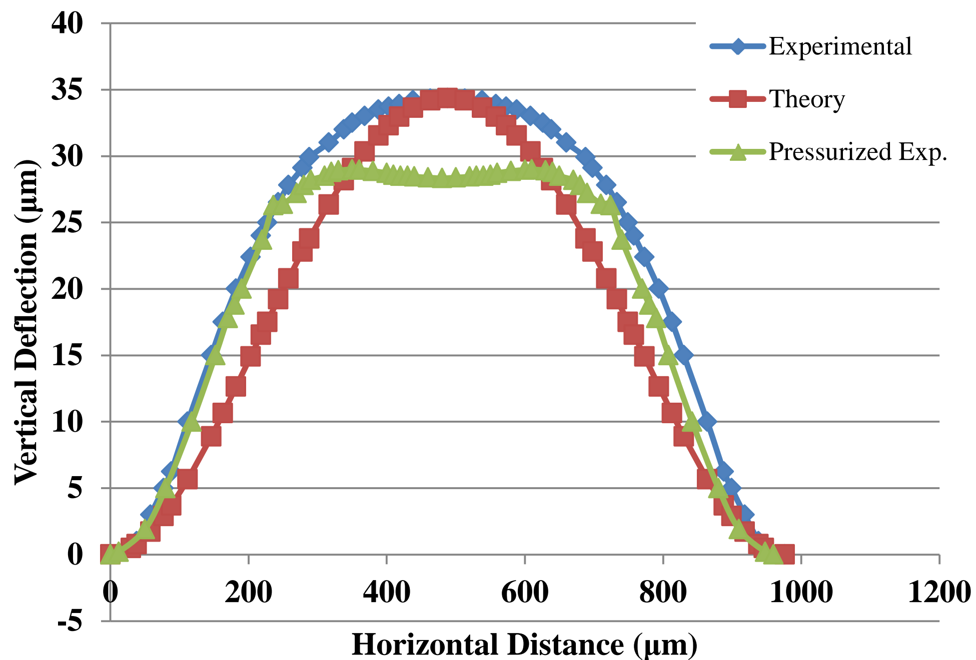

Figure 3. Vertical deflection curve of 900μm diameter membrane, comparison of theory, pressurized and un-pressurized experimental data [8].

In addition to buckled height and shape, the pressure at which the membrane switches from one buckled state to another, known as the actuation pressure, is derived from the same energy equations and assumptions originally made by Timoshenko. The actuation pressure of a diaphragm is a function of the deflection of the diaphragm and is given by the Euler-Bernoulli equation

$$D\nabla^4 w = p \tag{2}$$

where D is the flexural rigidity, w is the out-of-plane of the center, and p is the applied pressure. These two quantities, pressure and deflection, and how they compare to results obtained from finite element modeling are the focus of this work [9].

Schomburg *et al.*, [10], extended the theory into a more useable form. It has been modified to include effective properties of a layered model. The out-of-plane displacement of the middle of the diaphragm, w_c, is given by

$$w_c = \pm \frac{1}{8}\sqrt{-35\left(3\sigma_{eff}\frac{1-v_{eff}^2}{E_{eff}}R^2+4d^2\right)} \tag{3}$$

where σ_{eff}, v_{eff}, and E_{eff} are the effective residual compressive stress, effective Poisson's ratio and effective Young's modulus, respectively. R is the radius of the diaphragm and d is its thickness. The height just before actuation, w_{snap}, is given by

$$w_{snap} = \pm \frac{1}{24}\sqrt{-105\left(3R^2\sigma_{eff}\frac{1-v_{eff}^2}{E_{eff}}+4d^2\right)} \tag{4}$$

When the argument of the radical becomes imaginary, buckling is theoretically not possible at a ratio of radius to thickness

$$\frac{R}{d} \leq \sqrt{-\frac{4}{3}\frac{E_{eff}}{\sigma_{eff}\left(1-v_{eff}^{2}\right)}} \tag{5}$$

Finally, the actuation pressure, p_{act}, to switch the membrane is given by

$$p_{act} = 4\frac{w_{snap}\,d}{R^2}\left(\frac{4}{3}\frac{d^2}{R^2}\frac{E_{eff}}{1-v_{eff}^2}+\sigma_{eff}+\frac{64}{105}\frac{w_{snap}^2}{R^2}\frac{E_{eff}}{1-v_{eff}^2}\right) \tag{6}$$

It is interesting to note that actuation pressure is independent of direction. Switching "up" or "down" is denoted by the ± in equations (3) and (4). The actuation similarly only changes sign depending upon the switching mode [10,11].

Timoshenko [7] also considered the buckling of a square plate. The development is similar to that of a circular plate. Ziebart, *et al.*[12], considered the mathematical buckling of a micro-fabricated square diaphragm, supported by a rigid substrate illustrated in Figure 4. They assumed in their model that the material of the diaphragm is isotropic with a constant in-plane pre-stress, σ_o, and is homogeneous.

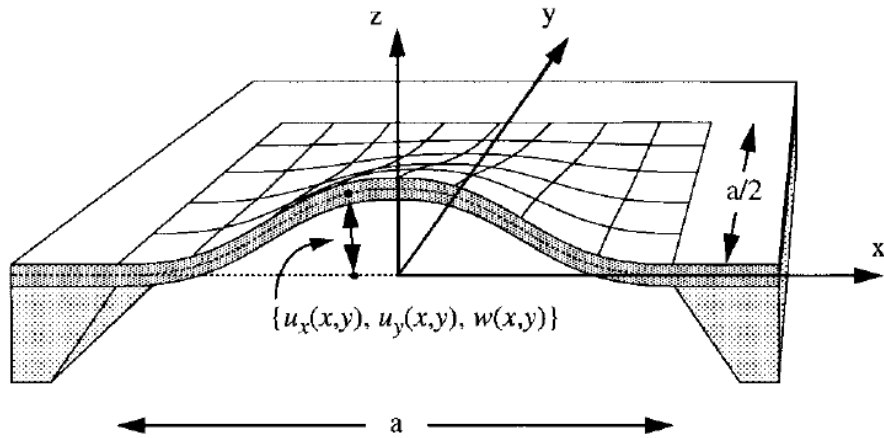

Figure 4. Cross-section illustration of a square, buckled diaphragm [12].

The isotropic etching process of the diaphragm can be clearly seen as the trapezoidal support structure under the diaphragm. The axes are defined on the neutral plane in the center of the diaphragm. They utilized an energy minimization method to calculate the shapes of the diaphragms. Figure 5 shows some of the experimentally determined higher-order buckling shapes.

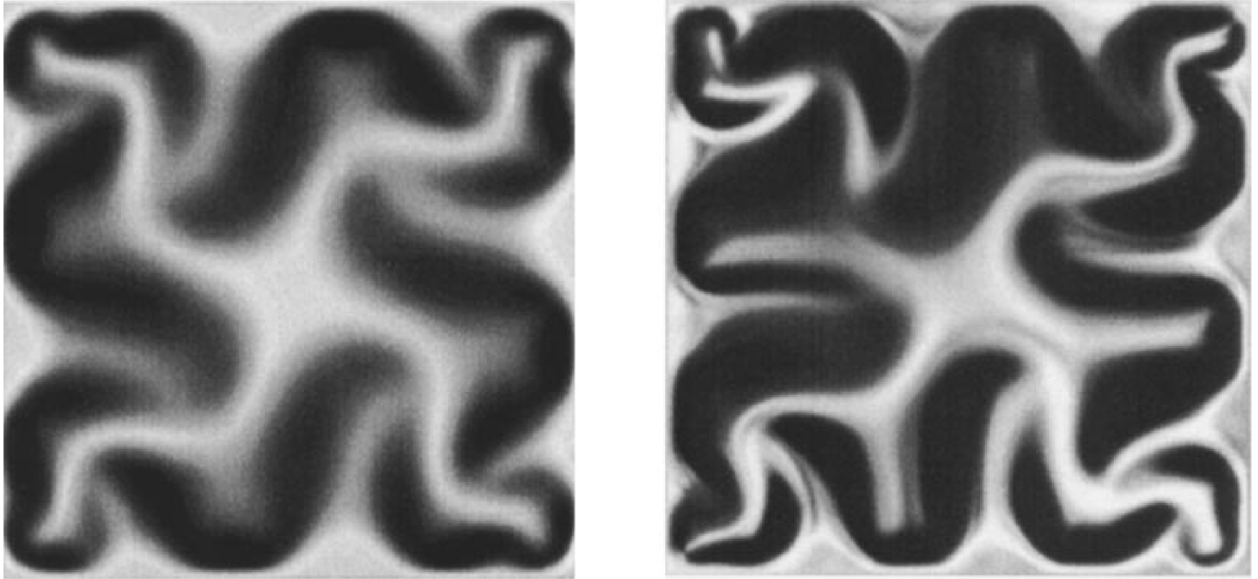

Figure 5. Buckled square diaphragms of different dimensions (side lengths: left 1425μm, right 1980μm). 1.0μm thick silicon nitride compressed with a stress of 61MPa [12].

The authors used a homogenous 1μm thick silicon nitride with a compressive stress of 61MPa and varied the length of the diaphragm to induce different buckling shapes. The larger diaphragms behave with high-order buckling modes as seen in Figure 5. The diaphragms for the work presented here are not completely homogenous, since polyimide is deposited onto silicon dioxide [12].

The authors then conducted a finite element analysis (FEA) of their diaphragms using ANSYS with an element type of Shell 63. Similar to the process used in this work, they simulated the pre-stress of the diaphragm using a thermal load [12]. Because other

thermal effects are not considered throughout the rest of the experiments, an actual coefficient of thermal expansion is not required, and a temperature that results in the measured pre-stress is sufficient. They loaded their FEA model similarly to the procedure in this work as well to find the first buckling shape. A small pressure was applied to the diaphragm; the thermal loads were then slowly applied; and finally the pressure was slowly removed. This roundabout process bypasses numerical instability in the FEA model [12]. The process in this work follows a similar path and is elaborated in the procedure section. The authors did note that the discontinuous shape function derivatives in the FEA model may lead to error. Figure 6 shows the finite element solution of the buckled profile of the diaphragm plotted against the normalized side length of the diaphragm. As the size of the diaphragm is increased, the degree or severity of buckling increases resulting in a larger center deflection (vertical axis of the graph). The smaller diaphragms show a uniform, parabolic buckled shape for a small value of w, higher-order modes are seen as the diaphragms get larger [12].

They note that the boundary conditions of the fabricated devices may account for the discrepancies in the profiles, which become more pronounced at the edges. Micro-fabrication processes can result in undercutting of a feature. Fabrication variations result in irregular boundary conditions. Similar to the work presented here, Ziebert *et al.* used a compressive stress of about 61MPa to cause buckling in diaphragms of approximately the same size used in this work [12].

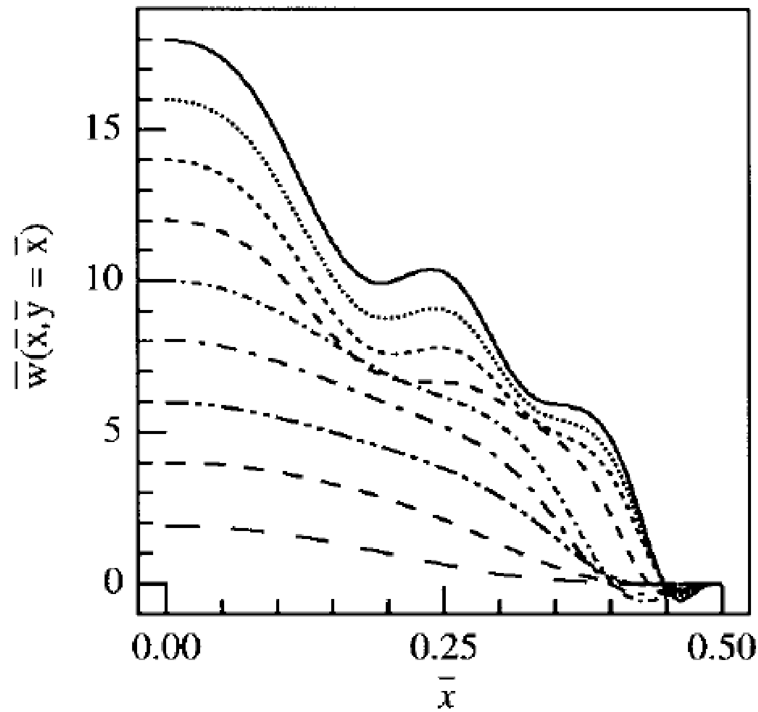

Figure 6. Finite element simulation of the buckled profile along the diagonal, symmetry about the middle. The horizontal axis is the normalized side length of the square diaphragm. Each line represents a different size diaphragm. As the diaphragm size increases, higher order buckling modes are seen [12].

In-plane strain piezoelectric properties of lead zirconate titanate (PZT) are of interest for the actuation of membranes without the use of pressure. This was the case studied by Ayela *et al*. [13]. They conducted a study on a circular diaphragm with a protrusion in the middle of the diaphragm to determine these properties of PZT. Figure 7 is their finite element model of the diaphragm in CoventorWare, a micro-fabrication process simulation and bundled FEA software package. Their goal was to determine the piezoelectric properties of materials by causing the diaphragm to buckle, which occurs when the radial compressive stress is greater than the critical radial force. The critical radial force for buckling, *Ncr*, was determined with

$$N_{cr} = k\frac{D_2}{R_2^2} \tag{7}$$

where k is constant dependent upon the relationship of the two radii, D_2 is the equivalent stiffness, and R_2 is the outer radius of the diaphragm. Similar to the work done by Ziebert, *et al.* [12], Ayela, *et al.*, assumed that each layer is transversely isotropic and a constant thickness, that the plate experiences only plane stress normal to z, and that the material is linearly elastic. They observed close results between their analytical model (which extended Timoshenko's and Krieger's work, Theory of Plates and Shells [7]), and a finite element model. However, best results were observed when the radius of the protrusion was less than or equal to 70% of the radius of the whole diaphragm [13].

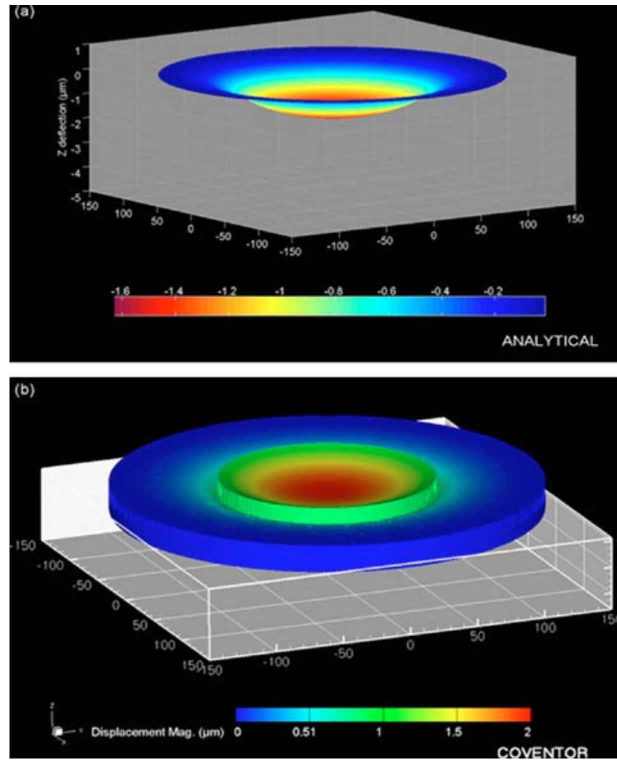

Figure 7. Comparison between analytical and finite element model of Ayela *et al* [13].

Ultimately they focused on having the radius of the protrusion fixed at 75μm and the outer radius of the diaphragm fixed at 200μm. By adjusting the thickness of the silicon diaphragm the amount of deflection calculated is shown in Figure 8. The study focused on creating an analytical model of a multi-layer device, and was able to report good agreement between their analytical and finite element models as shown in Figure 9 [13]. The x-axis of the figure is the ratio of R1/R2 or the relationship between the radius of the protrusion and that of the diaphragm. The y-axis is the amount of deflection of the diaphragm [13].

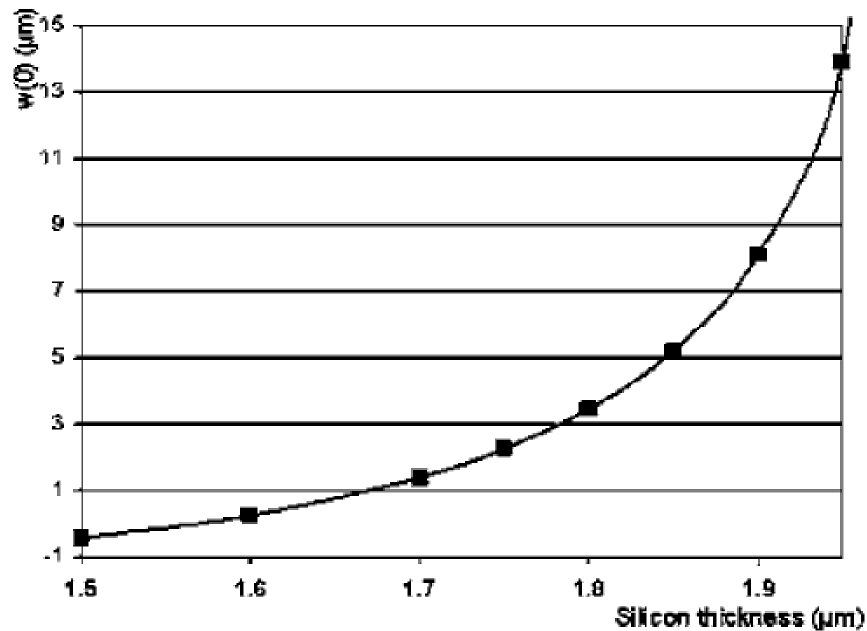

Figure 8. Silicon diaphragm thickness versus calculated deflection of the diaphragm out of the plane [13].

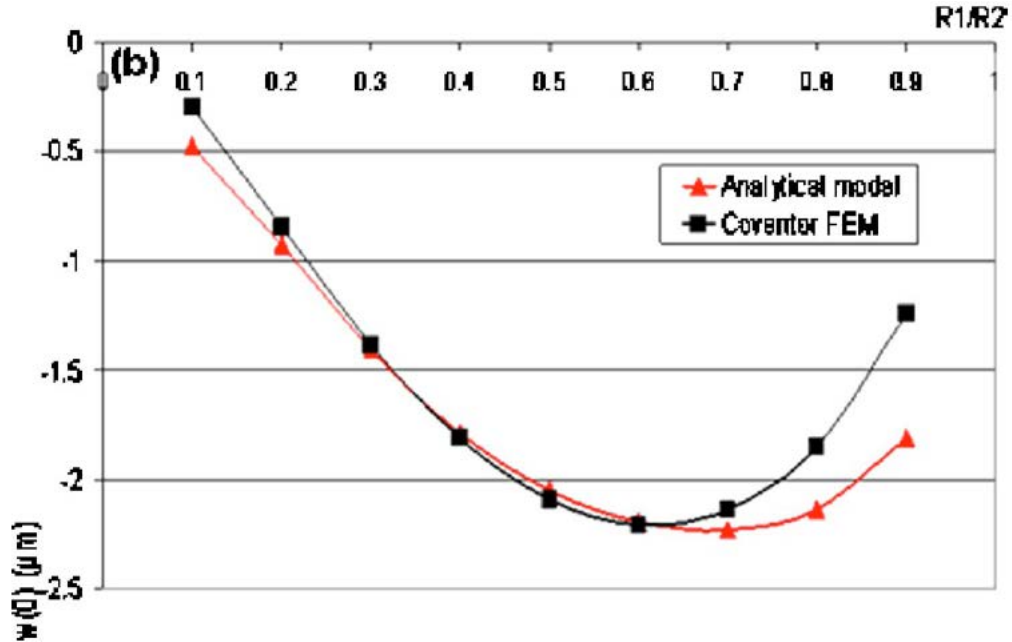

Figure 9: Comparison of analytical and finite element data [13].

Although the work presented by Ayela *et al.* is mostly concerned with the deflection of the diaphragm and not as much with the actuation pressure, it does offer some insights into the behavior of multi-layer diaphragm systems. Additionally the presence of the protrusion complicates the model in comparison to the work done in this paper. Therefore, high resolution measurements of diaphragm displacement can be translated into accurate actuation pressure estimation.

Gowrishetty *et al.* [14], worked extensively at the University of Louisville in the fabrication and testing of circular bi-stable buckled membranes. Silicon dioxide was grown on a (100) silicon wafer using wet oxidation until a thickness of 400nm was achieved. The diaphragm windows were etched from the backside, leaving only a thin silicon dioxide diaphragm. Polyimide PI-2610 was then spun onto the top surface of the diaphragms. Only 300μm diaphragms were fabricated, an image of one is shown in Figure 10. These parameters led to a bi-stable device that would buckle either up or

down. The authors observed a buckled height of about 7.6µm for both up and down. The authors assumed that the stress from the polyimide layer had a negligible effect on the device. They confirmed this assumption by noticing that the diaphragms did not favor a buckling state, but appeared to be random. Random buckling indicates the buckling follows the traditional mechanics of materials buckling of a homogeneous beam. An analytical model developed by Schomburg *et al*. [10] predicted an actuation pressure of 60kPa, where the authors only observed an actuation pressure of 41kPa. They concluded that the discrepancies were most likely due to variations in the fabrication of the devices [14].

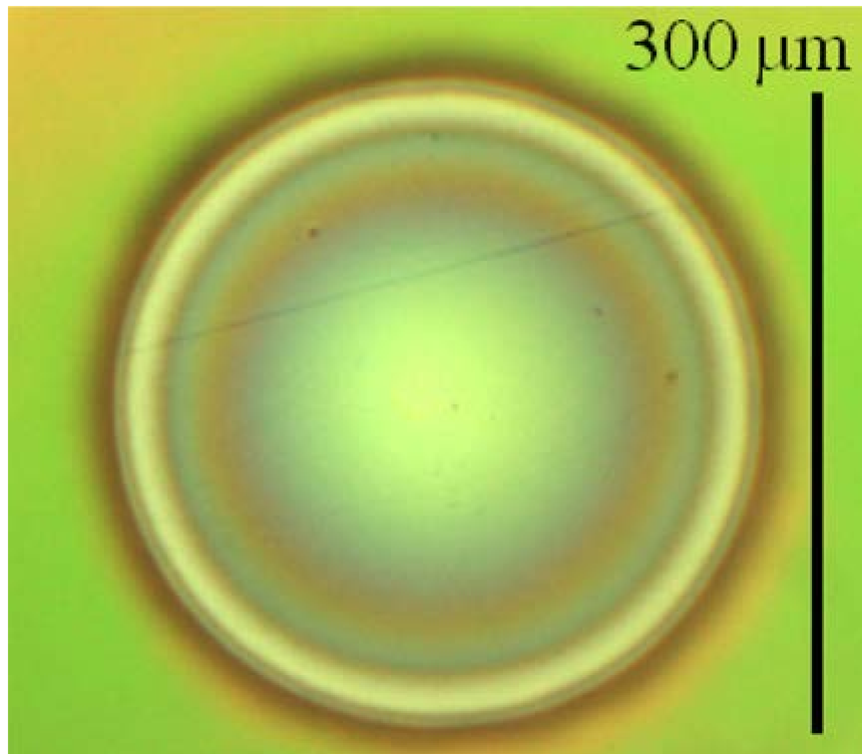

Figure 10: 300µm diameter diaphragm from Gowrishetty et al. [14].

II. PROCEDURE

A. Fabrication

The micro-fabricated diaphragm devices were produced on substrates of <100> oriented silicon wafers with an approximate thickness of 300μm. The initial (bare) wafer curvature was measured and recorded on a ToHo FLX-2320-S Film Stress Measurement System. Silicon dioxide was then grown thermally to a thickness of 450nm by wet oxidation in an oven at 1000°C for about one hour. The wafer curvature was re-measured using the same system and by Stoney's equation the residual compressive stress was determined. Stoney's equation is given by [15],

$$\sigma = \frac{E_s\,(t_s)^2}{6\,t_f\,(1\text{-}v_s)}\left(\frac{1}{R}-\frac{1}{R_o}\right) \tag{8}$$

where σ is the residual stress; E_s is the Young's modulous, t_s is the thickness, and v_s is the Poisson's ratio of the substrate respectively; t_f is the thickness of the of the film; R_o is the radius of curvature of the bare silicon wafer; and R is the radius of curvature of the wafer with the film. This equation is valid for $t_f << t_s$. The thickness of the silicon dioxide is 0.4μm compared to the thickness of the silicon wafer of 300μm; therefore this equation is valid. From equation (8) and the measured change in curvature, the residual stress in the SiO_2 film is 300MPa. PI-2611 polyimide from HD Microsystems was spun onto the wafers and cured to a thickness of 3.8μm after 7 hours in a Yield Engineering Systems high temperature oven. Photoresist was spun onto the backside of the wafer and the diaphragm design was patterned onto the back. Next, the wafer was placed in buffered

oxide etch (BOE) to remove the exposed SiO_2. Finally, the wafer was placed in an STS MESC Multiplex ICP to etch, by deep reactive ion etching (DRIE), through the silicon substrate up to the diaphragm SiO_2 layer. The DRIE process is also used to separate each die from the wafer [11].

Figure 11. L-Edit mask layout for the 100mm diameter wafer.

The wafer layout that was used to create the diaphragms is in Figure 11. Each die is represented by the small rectangles. The numbers within the die are the sizes of the diaphragms on the die in microns. The large red circle is a representation of the wafer.

The two dies with plus signs are used for alignment purposes. The large black cross in the middle is a center mark and was not a part of the mask. The four arrays above the center mark have a close spacing and will be referred to as "close arrays", and correspond to array 1 and array A and were tested extensively. These arrays mimic the dimensions used by Porter *et al* [11]. Dies B, C, and D, which were also tested, were located further from the center of the array.

B. Pressure Testing

The initial buckled heights of the diaphragms were measured in the clean room using a Veeco Dektak 8M profilometer. The tip of the profilometer traveled the entire diameter of each diaphragm while using the smallest possible force of 6.9μN. Actuation pressure testing of array 1 using the old test fixture from Gowrishetty et al. can be seen in Figure 12.

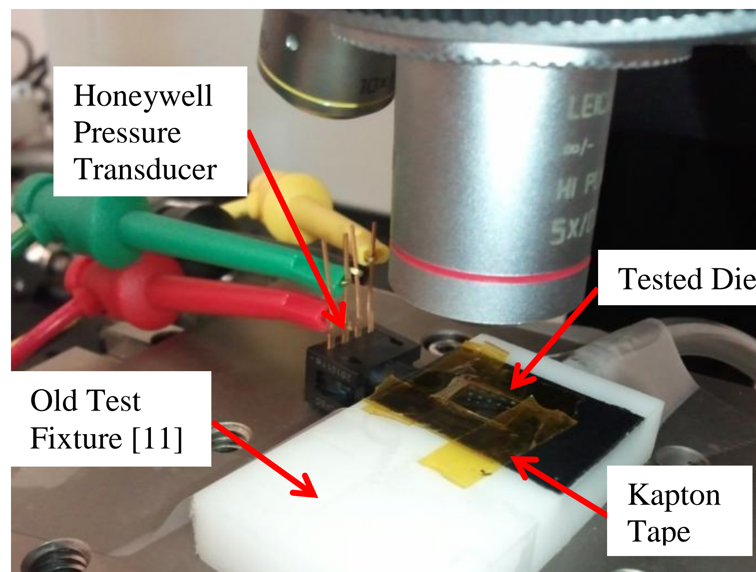

Figure 12. Array mounted in old test fixture with pressure sensor connected. Test fixture from [11].

Pressure is applied to the array using a barbed fitting and soft PVC tubing. Kapton tape is used to seal the die to the test fixture. The use of tape can damage the die if the tape is not removed carefully. Secondly, only the vacuum pressure switching mode is feasible, since the vacuum pressure reinforces the seal of the tape. Positive pressure applied to the fixture will cause the tape to release. A Honeywell 26PCCFH6G ±15 psig pressure transducer is mounted to the cavity below the array to measure the applied pressure. The pressure sensor is connected in a full a National Instruments (SCC-SG24) Wheatstone bridge module mounted in a National Instruments (NI SCC-68) module that is connected to a National Instruments NI M-Series Multifunction DAQ (NI PXI-6220) data acquisition card in a National Instruments (NI PXI-1033) PC module. Figure 13 illustrates the data acquisition system and test process schematic.

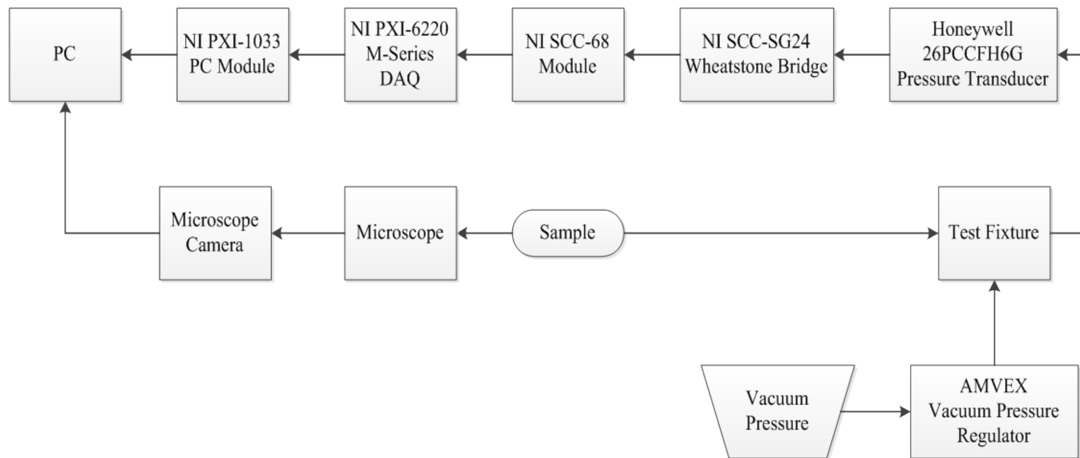

Figure 13. Test process schematic.

As the test process schematic shows, a sample is placed in the test fixture that has regulated vacuum pressure applied and is monitored by a data acquisition system. The microscope directly views the sample and the image is recorded via the microscope

camera. Figure 14 shows the Wheatstone bridge and NI SCC-68 module that were used. Regulated vacuum pressure was applied to the bottom of the die in the fixture. An AMVEX Corp. medical vacuum pressure regulator was used to modulate the applied pressure. A LabView program was written to overlay the pressure data onto the image from the microscope that can be seen in Figure 12. Images were continuously recorded as the vacuum pressure was slowly increased. The images were captured with a frequency of about 1.2Hz. Figure 15 shows two consecutive images captured during a test. The bottom right diaphragm in Figure 15 is 700μm in diameter. The image clearly shows that the diaphragm switched from the “down” to the “up” state. Each switch was experimentally determined using this two-image technique.

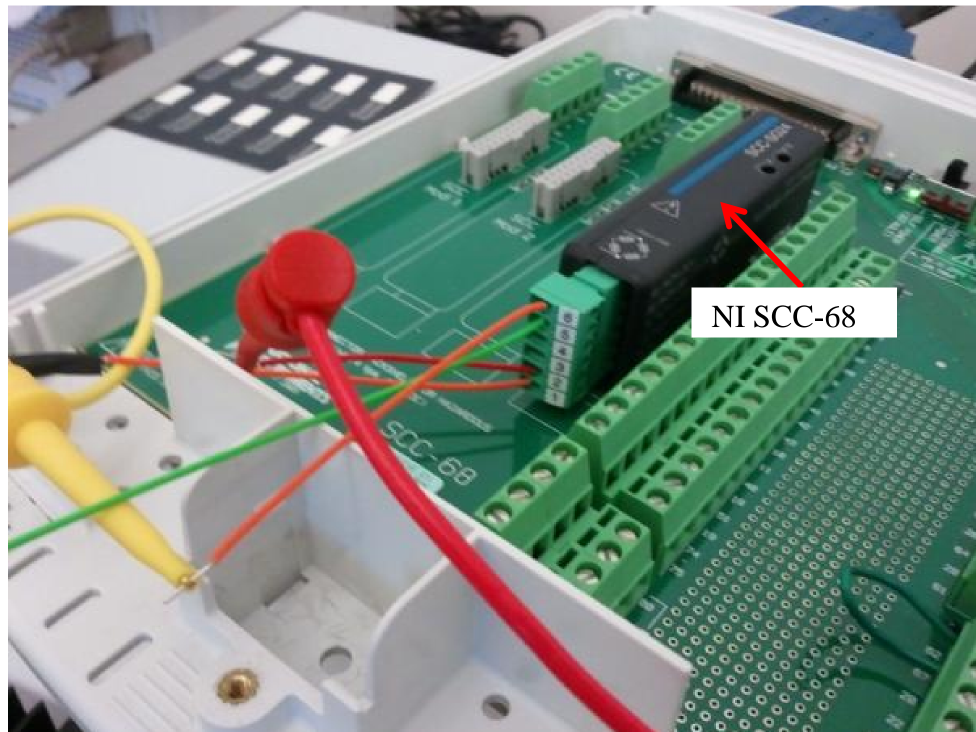

Figure 14. Wheatstone bridge and National Instruments module.

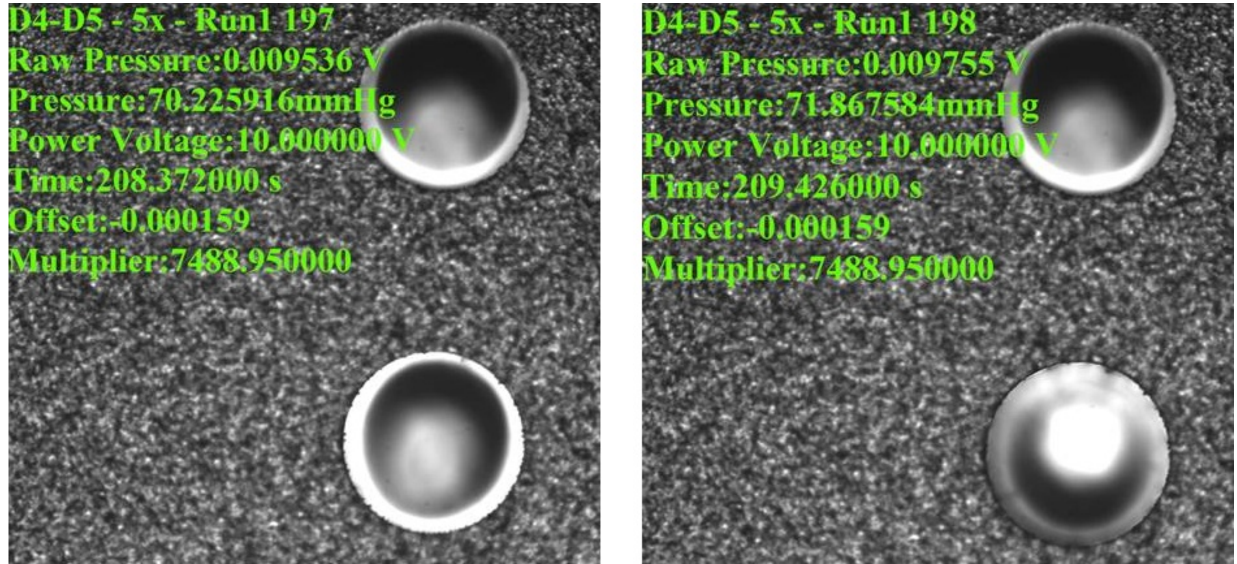

Figure 15. Consecutive images showing 700µm diameter diaphragm before switch (left) and after (right) viewed from the bottom of the die.

A new test fixture was developed and was created in the rapid prototyping lab at the University of Louisville. The solid model is shown in Figure 16. The green rectangle in the middle of the test fixture is a representation of a die. O-rings are mounted in the top and bottom portions of the fixture. The O-ring groove is illustrated in Figure 17. A similar groove is also on the underside of the top portion of the test fixture. The die is supported between two O-rings for a uniform seal on the die. Bolts are put through the holes and nuts are hand-tightened down to apply pressure to the O-rings to create the seal on the sealing surface. The hole on the side of the fixture is threaded for the Honeywell pressure transducer. Finally, the barb on the front face of the test fixture is fitted to the PVC pressure line used in testing. This barb opens onto the cavity under the die. By utilizing the barbed fitting the test fixtures were interchangeable within the set-up. The actual test fixture is shown in Figure 18.

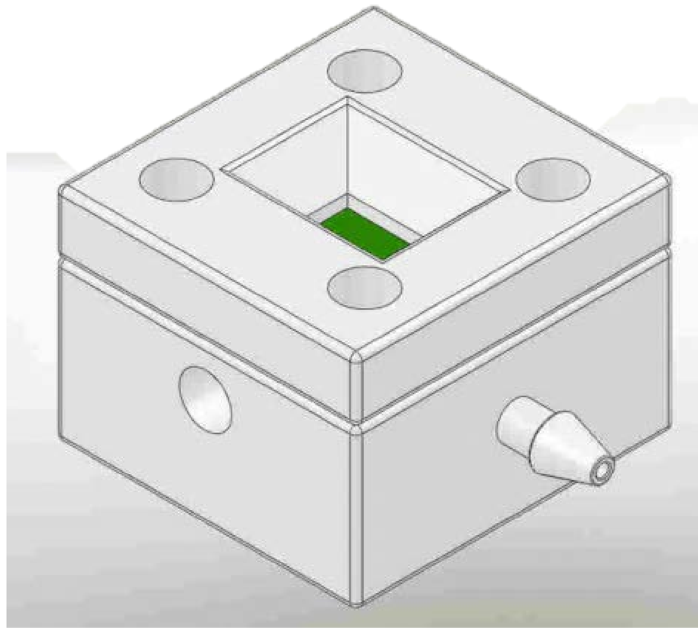

Figure 16. New test fixture solid model.

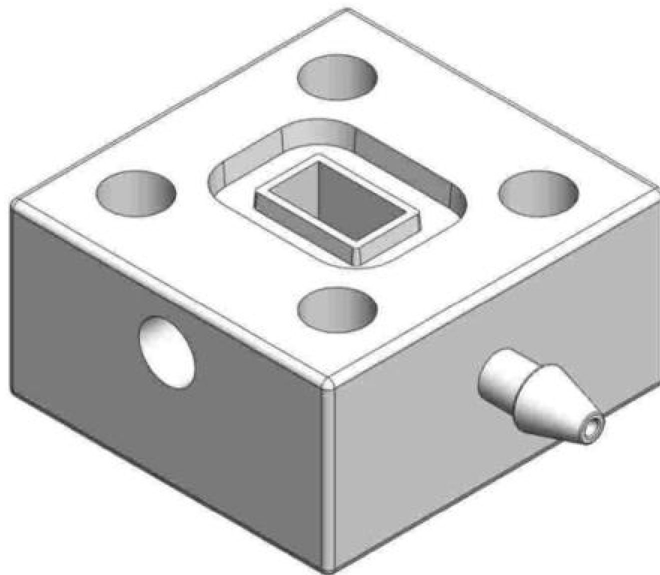

Figure 17. Bottom section of the new test fixture.

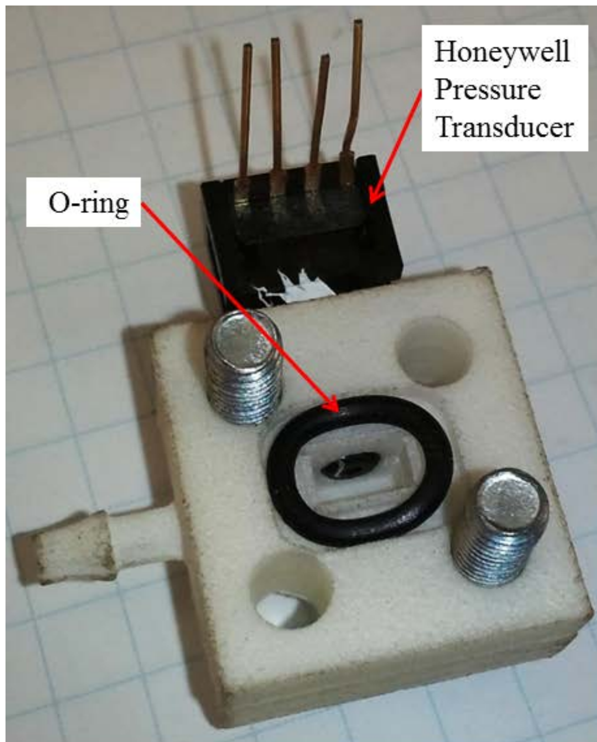

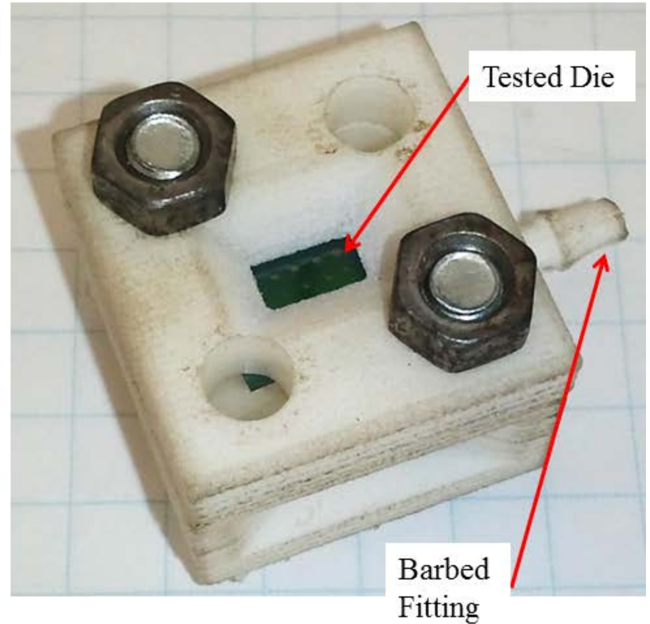

a) b)

Figure 18. New test fixture with component callouts: (a) bottom section, (b) assembled fixture.

The bolts compress the two O-rings around the die and seal to the cavity under the die. This cavity connects directly to the pressure transducer and the barbed fitting for the pressure source. The design used here is suitable for both vacuum pressure and positive pressure switching.

C. ANSYS Simulation

ANSYS 14.0 was used as the finite element modeling software. An axisymmetric model of shell 209 elements was used. A parameterized script file was generated to run each diaphragm diameter the same. Figure 19 shows the element plot of the right end with all degrees of freedom (DOF) fixed.

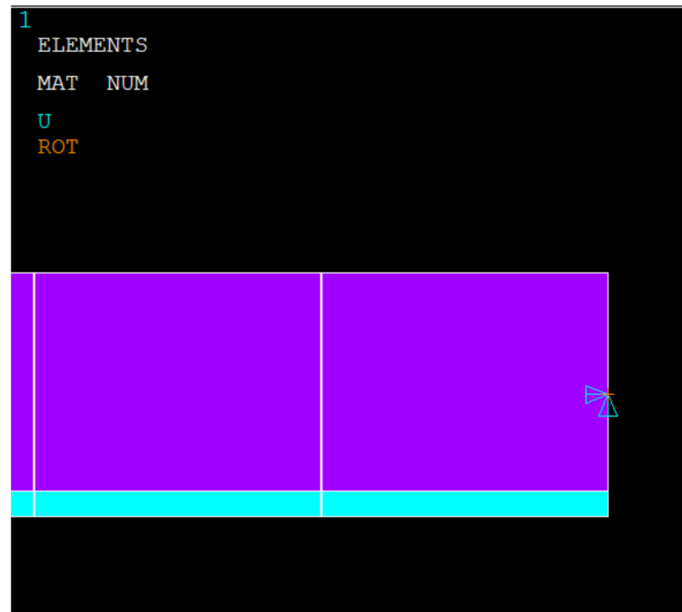

Figure 19. Element plot showing boundary conditions at right end.

The purple material in Figure 19 is the polyimide and the blue material is the silicon dioxide. The two triangles at the right indicate that both axial and vertical displacements are zero. The orange symbol at the intersection of the triangles indicates that in-plane rotations are also zero. The left end, located at the origin, is similarly constrained except it can move vertically. The representative complete element plot is shown in Figure 20, each diaphragm size was modeled using 100 elements and is constrained the same way.

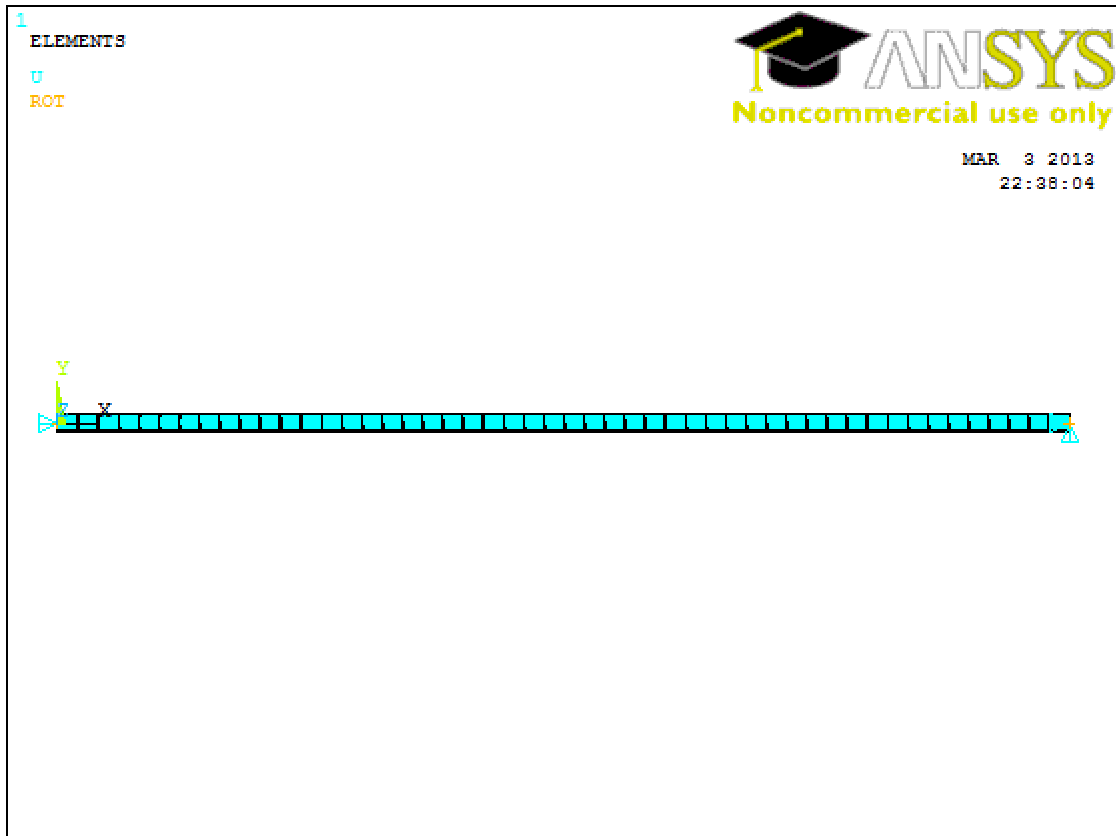

Figure 20. Element plot of axisymmetric shell model. Left keypoint constrained to not move horizontally or rotate about z. Right keypoint constrained in all directions.

The left end is constrained to not move in the x-direction or rotate about the z-axis. These boundary conditions equate to symmetry about the y-z plane. A quarter symmetry expansion of the model is shown in Figure 21. The various colors on the contour of the diaphragm represent displacements in the y-direction. Red is the largest positive displacement and is at the center of the buckled up diaphragm in Figure 21 (a). For the buckled down case, the largest positive displacement are at the wall, shown in (b).

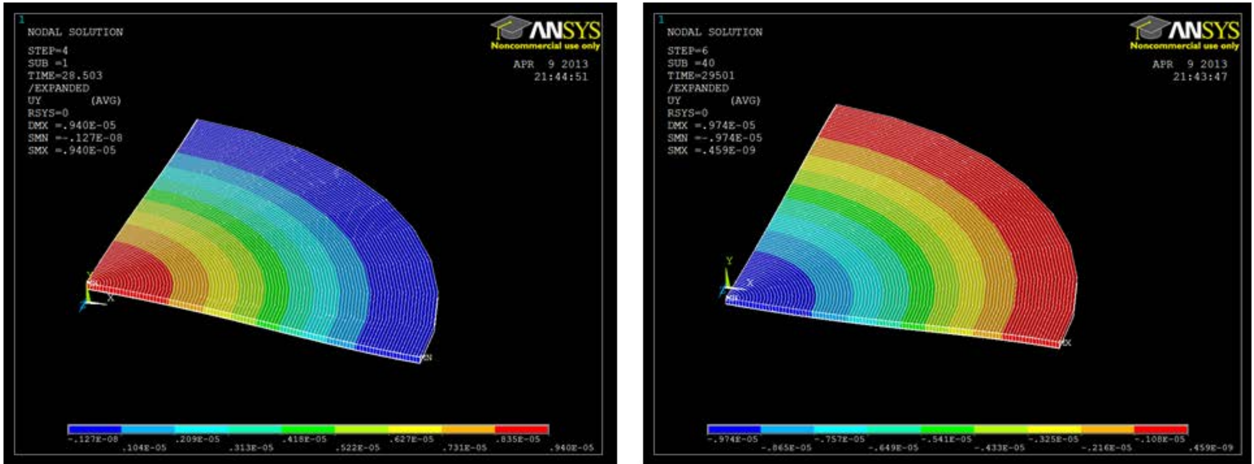

a) b)

Figure 21. Quarter symmetry expansion of Axisymmetric Shell209 model of 0.4μm SiO_2 and 3.8μm Polyimide layer, showing buckled up state (a) and buckled down (b).

The properties for the silicon dioxide and polyimide layers were determined from the literature. Silicon dioxide was assumed to have a Young's modulus of 73GPa and Poisson's ratio of 0.17. The polyimide was assumed to have a Young's modulus of 8GPa and Poisson's ratio of 0.20 [16]. The thickness of the silicon dioxide was found to be 400nm with a compressive stress of 300MPa. The polyimide was spun on at a thickness of 3.8μm. Other thickness of polyimide were tested, 2.5μm and 4.5μm with a compressive stress of 320MPa. These alternate designs were produced by Gowrishetty *et al.* [8]. The stress in the polyimide layer was tested by changes in wafer curvature and equation (8), and was consistently found to be negligible, since the fabricated diaphragms were randomly buckled. The assumptions for the polyimide were confirmed by Gowrishetty *et al.* [8,14].

The compressive stress measured in the silicon dioxide layer is applied to the model as a temperature load. This methodology is well established in literature and mimics the compressive stress [12]. A section of silicon dioxide is modeled in ANSYS with Plane183 elements, mapped meshing, and is fully constrained, and axisymmetric. An element plot showing the boundary conditions of the thermal model is shown in Figure 22. A coefficient of thermal expansion is assigned to the material, in this case $4x10^{-6}$ m/m°C. The temperature is then ramped over a large range and the stress in the material is plotted using the Time History Post Processor in ANSYS. Figure 23 shows the graph of stress in the diaphragm section versus temperature. An applied temperature of 851°C results in a compressive stress of 300MPa.

Next, a complex series of load steps are applied. Figure 24 is a representative plot of the applied pressure versus the center displacement of the diaphragm, for the buckling down case. The first load step applies a small perturbation pressure to favor one buckled state. Then a temperature is applied to simulate the compressive stress in the SiO_2 layer. The third load step slowly removes the perturbation pressure and the first buckled state is achieved with no pressure load applied. The diaphragm is in a stable buckled state with the center of the membrane deflected up, or the initial buckled height, w_0. This condition represents the "as-released" state the diaphragms adopt following the completion of the micro-machining process. The fourth load step then ramps the applied pressure up to just before the diaphragm switches. The pressure is then increased very slowly over the actuation point and a little beyond in the fifth load step. The actuation pressure is obtained from looking at the resulting displacement graph such as Figure 24. Finally the

pressure is completely removed slowly and the second buckled state is achieved with no pressure load applied.

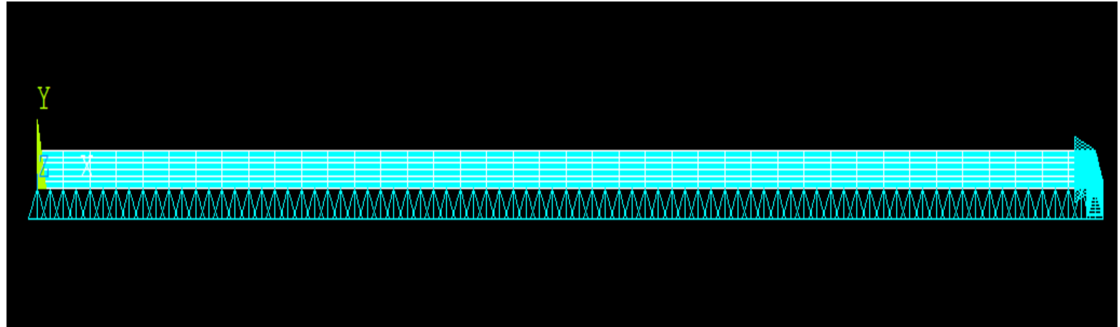

Figure 22. Element plot showing boundary conditions for thermal analysis of stress. Single layer of dioxide 0.4μm thick, 20μm long, axisymmetric.

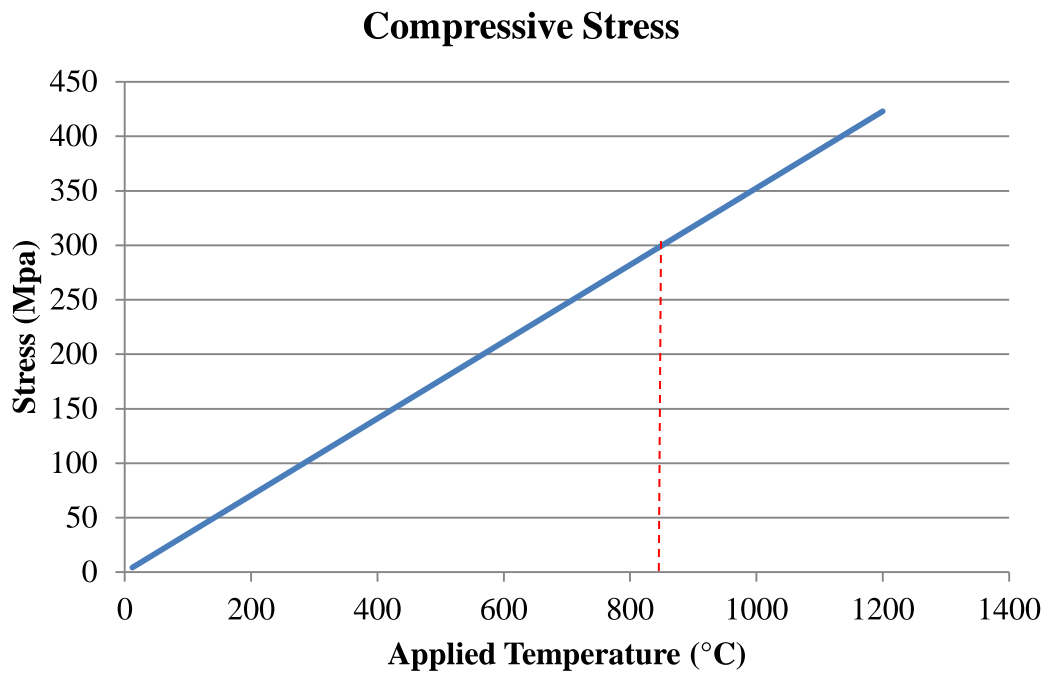

Figure 23. Stress versus temperature plot of ANSYS Plane 183 simulation.

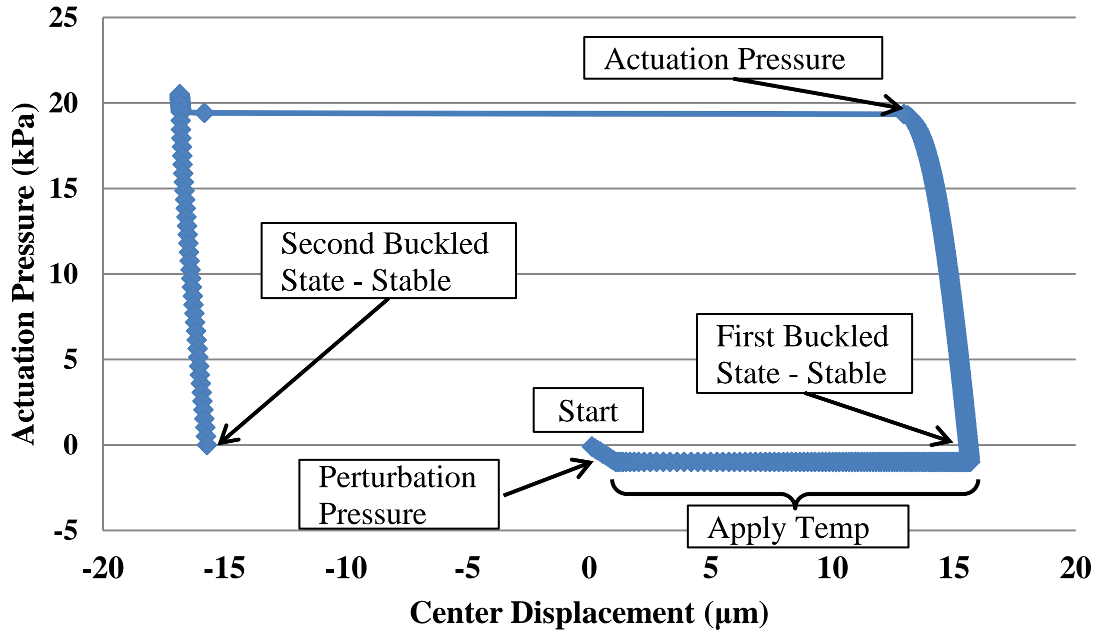

Figure 24. Representative ANSYS simulation loading plot, 600µm diameter diaphragm, buckling down.

The state of the diaphragm following the sixth load step is similar to its condition after the third load step. The new buckled state translates to the physical state of being buckled down, which is represented as a negative deflection in Figure 24. This same condition is reached experimentally by applying vacuum pressure to a diaphragm that is switched up, when the pressure is large enough to cause buckling, the diaphragm moves or snaps into its new state. Buckling up is achieved in a very similar process, except the perturbation pressure is positive, resulting in a negative displacement after load step three. Following load step six, the displacement is positive for the buckled up case.

III. RESULTS

A. Experimental Pressure Testing Results

Upon successful device fabrication, the majority of the produced diaphragms were found to demonstrate bi-stable buckling, switching between stable states under applied pressures as expected. Figure 25 is an image of the released dies after manufacture.

Figure 25. Released dies after manufacture – array 1 highlighted.

Array 1 (highlighted) clearly shows the successful production of a close patterned array. Array 1 was tested using the test fixture from Gowrishetty *et al*. shown in Figure 12. All of the other dies were tested using a newly designed test fixture which can be seen in Figure 16. The other dies are all present as well, although they are not yet labeled. The image was taken shortly after fabrication and the subsequent test specimens had not been identified specifically. Several of the manufactured dies were tested using the test fixture and methodology described above. Table 1 lists the tested dies and their descriptions. Dies B through D were fabricated to test the sensitivity of spacing diaphragms closely. The arrays fabricated by Porter *et al.*, [11], had been closely spaced. Dies B through D were fabricated with similar diaphragm sizes, but with large spaces between the diaphragms. Die E was fabricated to test how a larger aspect ratio affected the buckling performance. Refer to Figure 11 for graphical representations of the dies listed in Table 1. The diaphragms were switched up and down using vacuum pressure; this is illustrated in Figure 26.

Table 1. Description of tested dies

Die Name	Description
Array 1	Array of closely spaced diaphragms (20-900µm diameters)
Array A	Array of closely spaced diaphragms (20-900µm diameters)
Die B	Only 600µm and 225µm diaphragms
Die C	Only 650µm and 375µm diaphragms
Die D	Only 700µm and 250µm diaphragms
Die E	Only 1750µm and 1500µm diaphragms

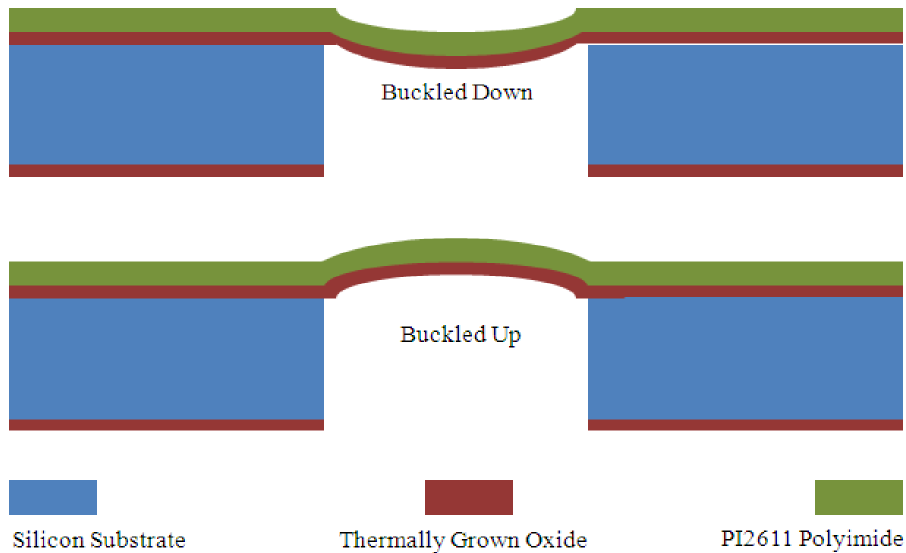

Figure 26. Graphical representation of switching modes.

Switching from the "up" state to the "down" state is called switching or buckling down and vice versa. The silicon beneath the smallest diameter diaphragms was not completely etched all the way through, resulting in the smallest diaphragms being unreleased. This effect can be seen in Figure 27. The highlighted diaphragms are much darker than the larger ones indicating that little to no light is allowed through. This indicates that the silicon was not completely etched. The topside of the array 1 is shown in Figure 28, which confirms the incomplete etching of the diaphragms. The dotted red circles show the region where the smallest diaphragms would appear if the etch had completely removed the silicon. No diaphragms with a diameter smaller than 200µm were ever etched successfully. Based upon the trends observed in the switching performance of the successful dies, the diaphragms with a diameter smaller than 200µm would not have been bi-stable. Therefore the arrays were not re-manufactured in the clean room.

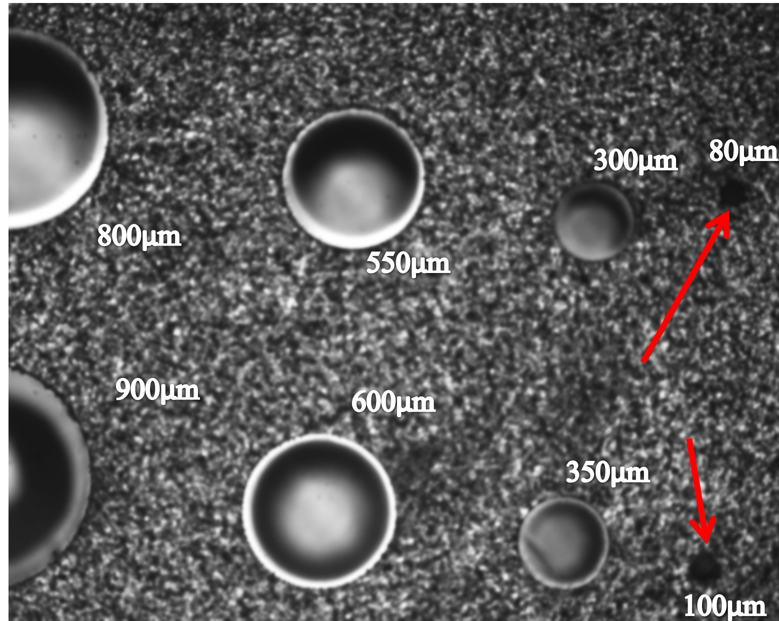

Figure 27. Backside of array 1 showing loss of smallest diaphragms (highlighted).

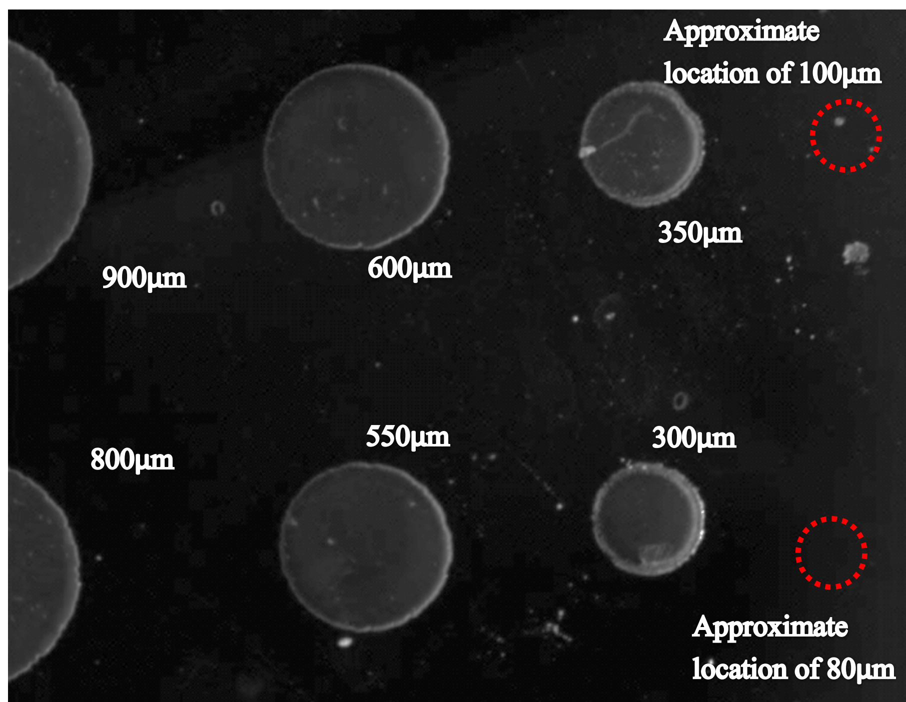

Figure 28. Topside of array 1, smallest diaphragms are not visible.

The vacuum pressure testing results for array 1 are plotted in Figure 29. The switching data trends downwards as the diaphragm size increases. This trend is mirrored in Figure 30, the switching pressures of array A. Both arrays behaved similarly. The switching pressure for the large diameter diaphragms was directionally independent as theory predicts. However, as the diameter decreases in size the actuation pressure becomes increasingly more dependent upon direction. The difference between array 1 and array A is the location on the wafer. The two share the dimensions and stress and show repeatability in device fabrication. The theoretical model is completely directionally independent and predicts the same actuation pressure regardless of direction, equation (6). Theory also predicts from equation (5) that the smallest diameter diaphragm that can switch from this configuration is 220μm. Fabricated diaphragms with a diameter 250μm or smaller would switch down, but they did not demonstrate bi-stability, they switched back up before all vacuum pressure was removed. The 200μm diaphragm on array A behaved this way, therefore only "down" data is available. This shows that the transition point of bi-stability was reached with these arrays. The data points represented here are averages across several runs of switching the diaphragms either up or down. The standard deviation in kPa is given for each of these graphs.

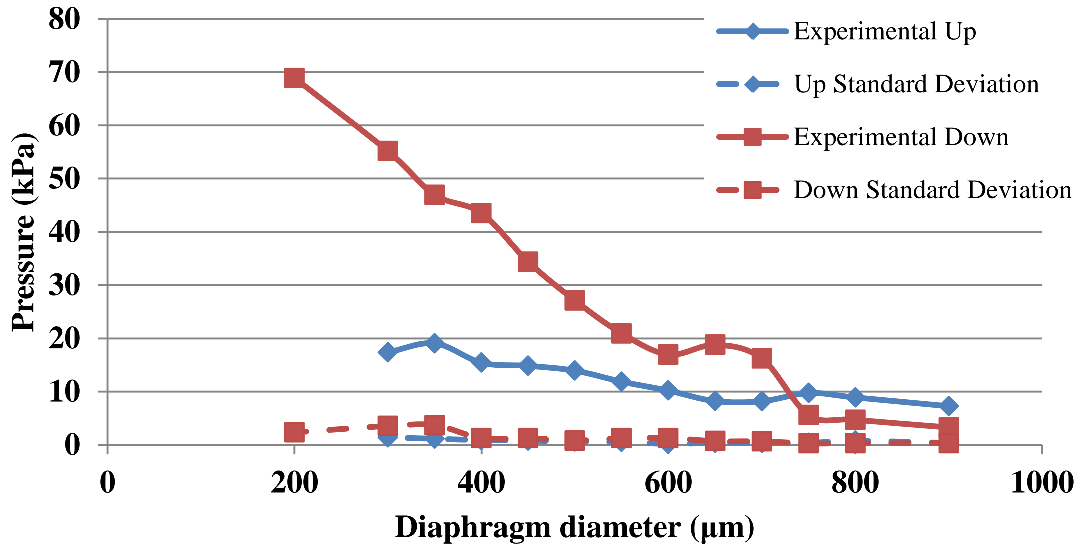

Figure 29. Array 1 experimental switching pressures. 300MPa compressive stress. Polyimide 3.8μm / SiO_2 0.4μm.

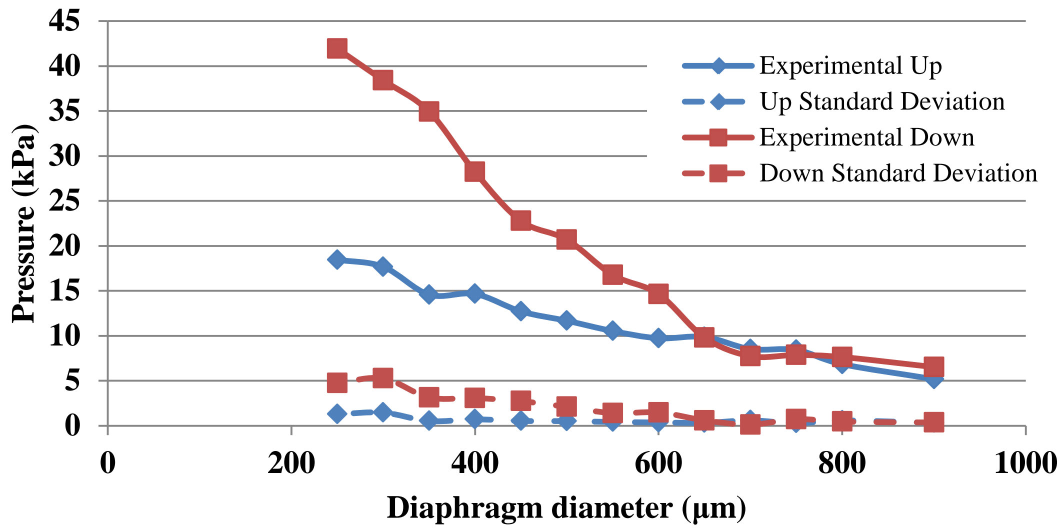

Figure 30. Array A experimental switching pressures. 300MPa compressive stress. Polyimide 3.8μm / SiO_2 0.4μm.

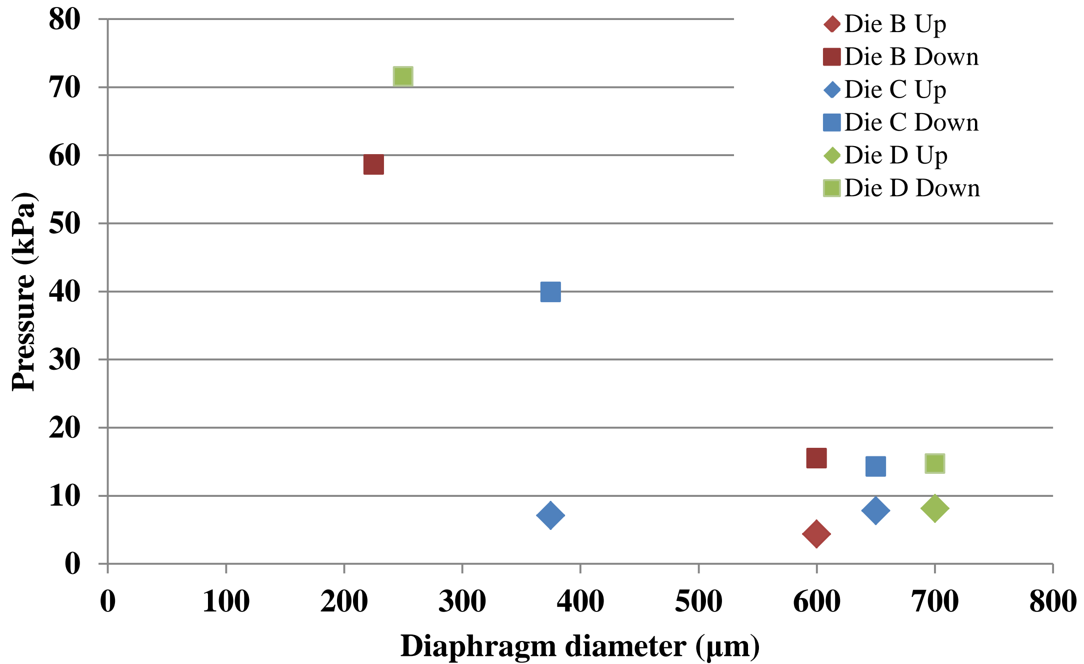

Figure 31. Experimental data from Dies B (600µm & 225µm), C (650µm & 375µm) and D (700µm and 250µm). 300MPa compressive stress. Polyimide 3.8µm / SiO_2 0.4µm.

Figure 31 is a graph of the pressure switching data for dies B, C and D. As with the arrays, the dies with only two diaphragms behave in the same fashion; the smaller diaphragms actuate at a larger vacuum pressure and the up mode does so at a lower value than the down mode, see Figure 36 and Figure 37 for a direct comparison. Diaphragms with a diameter of 250µm or smaller were initially buckled up when they were manufactured. However, these diaphragms were not bi-stable and buckled back up while there was still vacuum pressure applied. Switching up data for these small diaphragms is therefore not available. The standard deviation for these three dies is not plotted because all values were near zero and overlapped, their values are given in Table 2 for completeness.

Each die and array were tested several times and the pressure data results were averaged. Figure 32 shows the data points of the switching pressure of a 500μm diameter diaphragm from array 1. The run number corresponds to the number of the test. The testing method captures a picture before and after actuation. The pressures from these two pictures are reported here with the corresponding average. At least 3 tests or runs were performed on each diaphragm for each die. Frequently more runs were performed, this is reflected in Figure 32 with multiple run numbers. The runs are averaged together and the result is plotted in the actuation pressure plots. Similar plots could be generated for each diaphragm, but are only reported as averages, since the data is fairly consistent between runs.

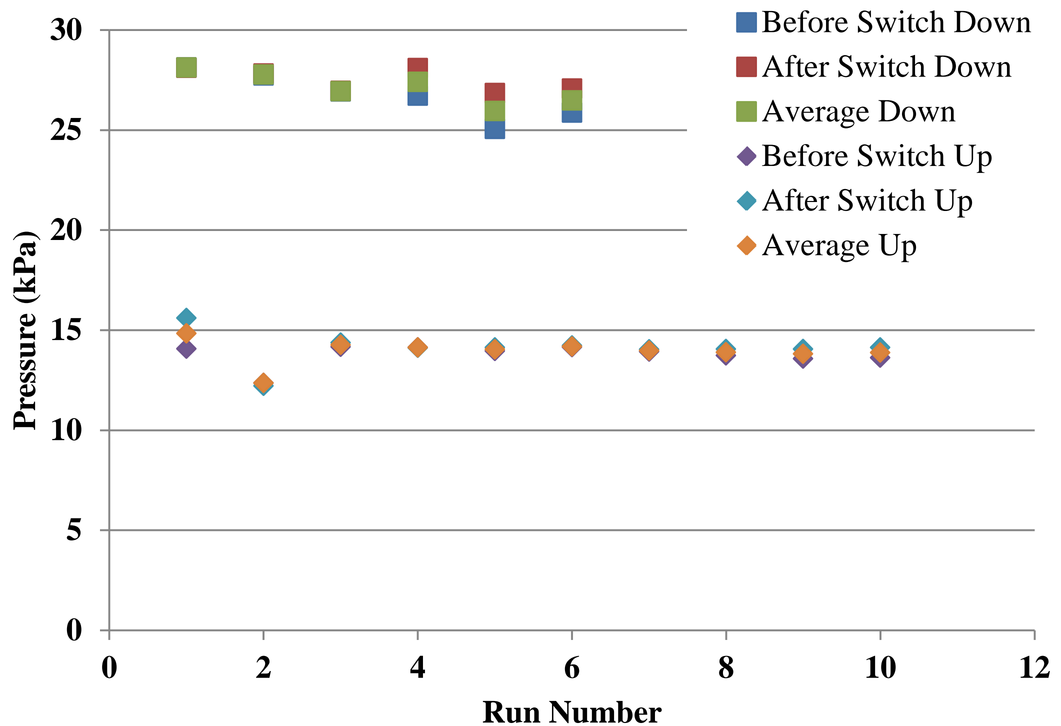

Figure 32. Complete actuation data for a 500um diameter diaphragm from array 1 showing repeatability between successive runs. 300MPa compressive stress. Polyimide 3.8μm / SiO_2 0.4μm..

Table 2. Standard deviation of dies b, c, and d used in experimental testing.

Die	Diaphragm size(μm)	Down	Up
B	600	0.409	0.413
	225	0.912	-
C	650	0.146	0.550
	375	0.477	0.473
D	700	0.540	1.278
	250	1.033	-

B. ANSYS Modeling Results

The ANSYS data was gathered from plotting the applied pressure versus the displacement of the center of the diaphragm similar to Figure 24. The buckled heights of the diaphragms and the actuation pressures were determined from the data that generated the plots. The larger diaphragms were very unstable and would not always buckle sharply, as the 600μm diaphragm did in Figure 24. The inherent instability of a large diaphragm, 1500μm, is illustrated in Figure 33. The diaphragm center, shown in Figure 33, starts at the left most end of the blue line, near (0,0). A small perturbation pressure of 1000 psi is applied slowly for a displacement of about 10μm. Compressive stress is then simulated using a temperature which ramps until the compressive stress is reached. The perturbation pressure is then removed, and the diaphragm reaches its stable buckled height of about 35μm. Finally, a positive pressure is applied and ANSYS calculates the new displacement using a modified Newton-Raphson technique. The pressure is ramped to a preset value, in this case 3.3kPa. The pressure is then removed and ANSYS uses the same technique to find the displacement. Figure 33 clearly shows the instability inherent

in such a large diaphragm. The diaphragm in this case did not snap-through or actuate. A large pressure must be applied to achieve actuation. ANSYS is seeking the lowest potential energy in the membrane and is using a modified Newton-Raphson technique to find the lowest energy. Figure 33 is an illustration of this search for the lowest energy. As more pressure is applied the solver finds the lowest energy by switching the membrane into the down configuration, negative displacement.

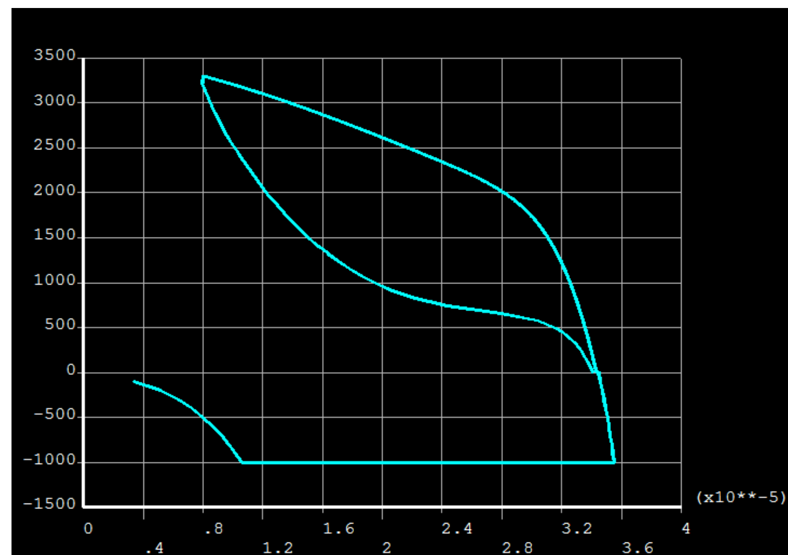

Figure 33. Buckling analysis illustrating inherent instability of a 1500µm diameter diaphragm. 300MPa compressive stress. Polyimide 3.8µm / SiO_2 0.4µm. (Vertical axis is pressure in Pascals. Horizontal axis is the displacement of the center of the diaphragm in meters.)

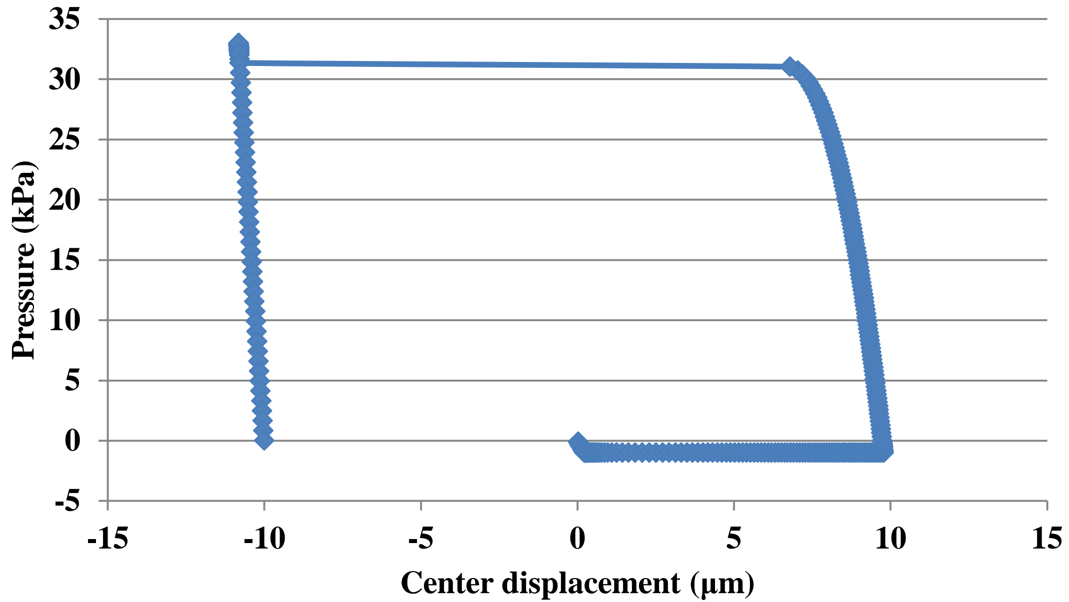

Figure 34. Successful actuation of diaphragm, 400 diameter. 300MPa compressive stress. Polyimide 3.8µm / SiO_2 0.4µm.

The case is rerun in ANSYS until actuation does occur. This same process is followed for each diaphragm size until the resulting graph resembles Figure 34, a successful actuation. The point of actuation is clear in this case. If the applied pressure is sufficient to cause actuation and does stop at the actuation point, all resulting graphs show clear actuation. Some larger diameter diaphragms have a more pronounced slope before actuation. This behavior is due to a dimple forming. Additionally, the smaller diameter diaphragms are much more stable and behave more linearly, and as theory predicts, refer to Figure 2. The steps as those used to generate Figure 33 were applied in the generation of Figure 34 as well. From the data points used to create these graphs, actuation pressure and buckled heights were gathered. Figure 35 presents the ANSYS actuation pressure data with actuation pressure data from array A.

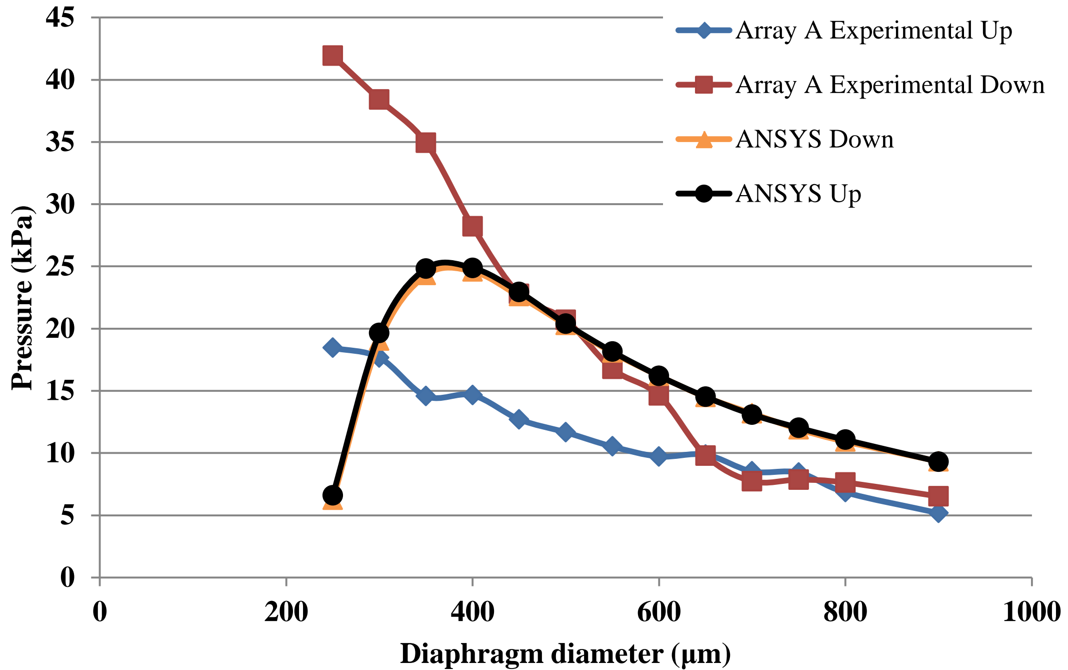

Figure 35. ANSYS FEA data and Array A experimental data. 300MPa compressive stress. Polyimide 3.8µm / SiO_2 0.4µm.

The ANSYS data follows the same trends as seen in the experimental data for the larger diaphragms. However, the data do not agree for the smaller diaphragms. The discrepancy is likely from un-modeled boundary conditions that become more pronounced as the diaphragms get smaller. Figure 36 plots all of the switching down data for the various dies except for die E and compares them to the ANSYS data.

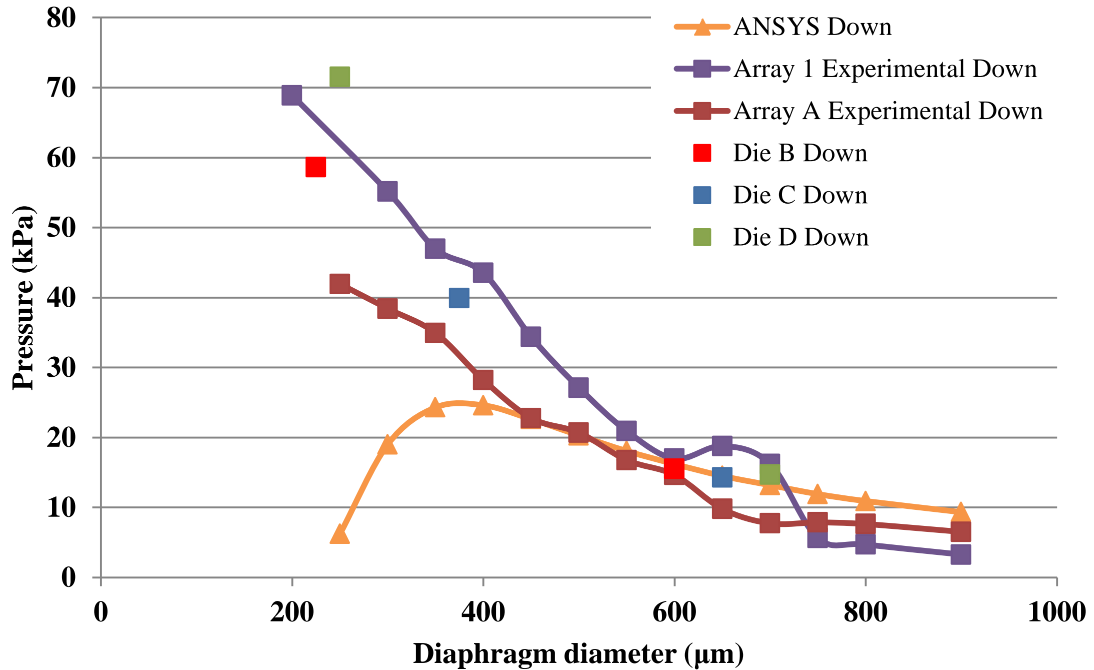

Figure 36. Experimental and ANSYS switching down data for tested dies and arrays. 300MPa compressive stress. Polyimide 3.8µm / SiO_2 0.4µm.

There is good agreement among all of the experimental data and variations are likely due to manufacturing processes. The minor differences between arrays 1 and A could come from the different fixtures used for testing. The largest variations are among the smallest diameter diaphragms which are most susceptible to variations in the DRIE process. Figure 37 is a similar plot to Figure 36, but for switching up data. Dies B and C both show very low data points in Figure 37, this is likely due to delamination or another directionally dependent effect. The ANSYS model consistently over-predicts the actuation pressure to switch the diaphragms up. Die E contains two very large diaphragms that were tested using the same processes; the switching data is presented in Figure 38.

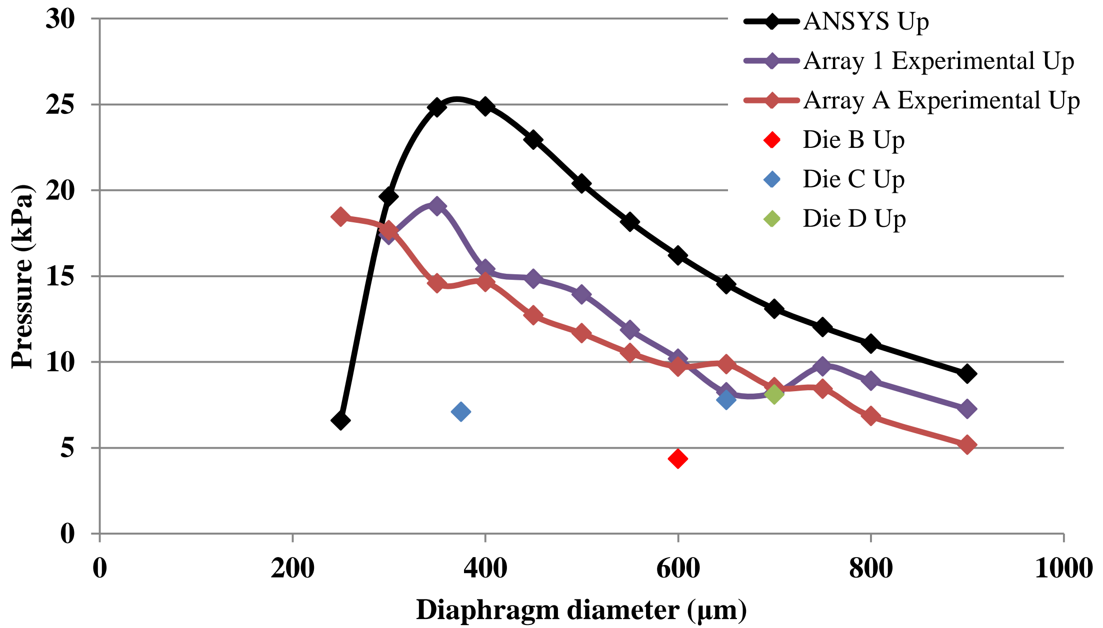

Figure 37. ANSYS and experimental switching up data for tested dies and arrays. 300MPa compressive stress. Polyimide 3.8µm / SiO_2 0.4µm.

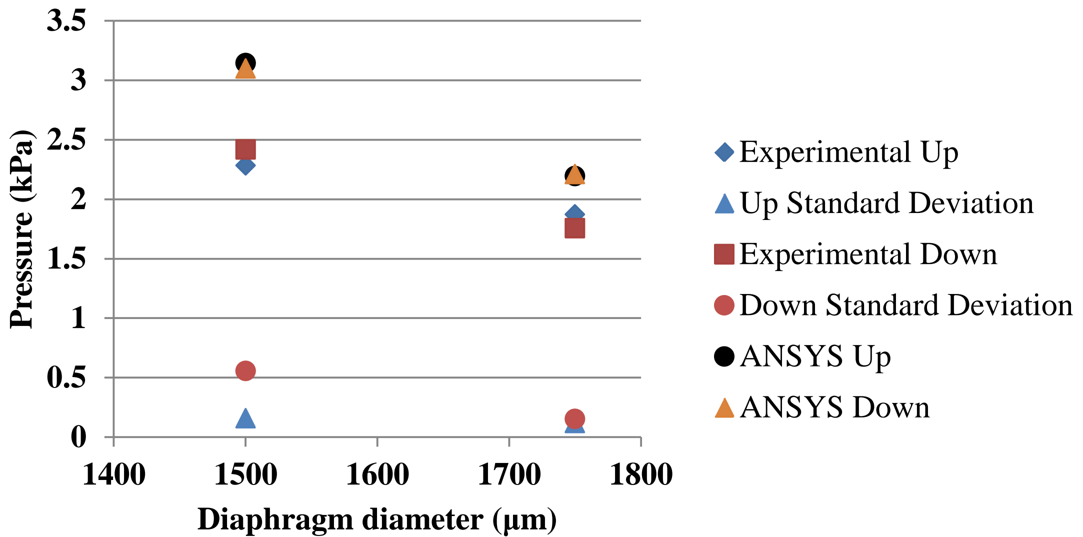

Figure 38. Die E experimental and ANSYS switching data. 300MPa compressive stress. Polyimide 3.8µm / SiO_2 0.4µm.

The data in Figure 38 follow the same trends the other switching data do. The ANSYS model over-predicts the switching pressure, and the experimental up and down data agree for these very large diaphragms.

In addition to actuation or switching pressure, initially buckled heights were measured and can be predicted using ANSYS. Figure 39 graphs the measured buckled heights for the various dies and the ANSYS data.

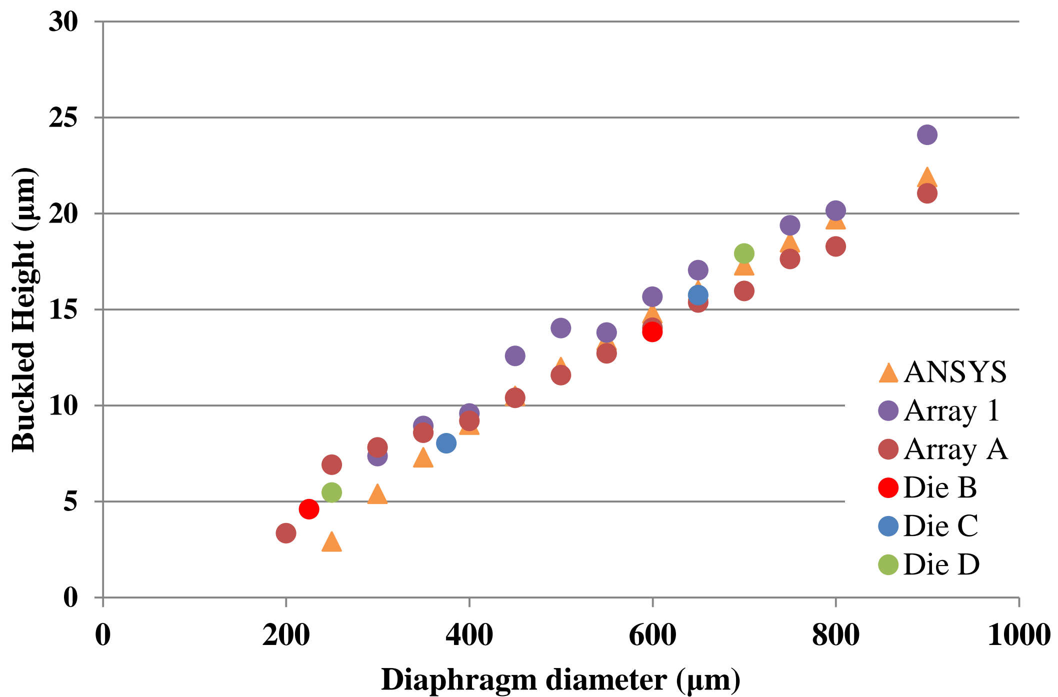

Figure 39. Buckled height comparison between ANSYS and experimental data. 300MPa compressive stress. Polyimide 3.8µm / SiO_2 0.4µm.

The data in Figure 39 clearly shows excellent agreement between ANSYS modeling and experimental data. The slight variations are likely due to manufacturing processes. Buckled height is also not as sensitive to boundary conditions as actuation pressures, since the smallest diaphragms are also in good agreement. Table 3 presents the buckled height data from die E in microns.

Table 3. Buckled Heights of Die E

Diaphragm size (μm)	1500	1750
ANSYS	33.72	38.03
Experimental	37.76	45.28

The buckled heights for die E (1500μm and 1750μm) are also in good agreement as they are in Figure 39. These values for die E were not plotted with others because the diaphragm sizes are much larger and the graph loses some of its detail.

IV. DISCUSSION

There are several possible reasons for the discrepancies between the ANSYS simulations and the experimental results. Theoretical modeling suggests, and ANSYS modeling confirms, that the actuation pressure should be independent of direction. One possible explanation is that the silicon dioxide and polyimide layers are delaminating from the silicon substrate. This is illustrated in Figure 40.

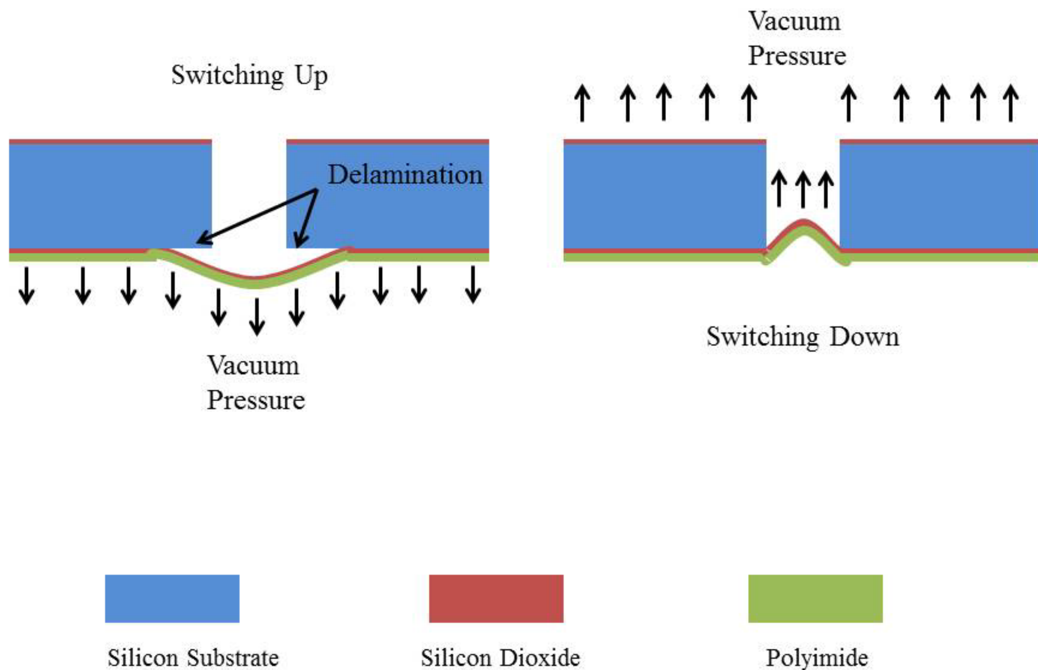

Figure 40. Delamination illustration for up and down switching modes.

The silicon substrate is able to support the diaphragm when the diaphragms are switching down. If delamination is occurring, that would explain why the actuation pressures in the downward direction are consistently lower, since it effectively makes the diaphragm larger. For a larger diaphragm, a small increase in effective diameter will only have a minor impact. However, the same amount of increase for a smaller

diaphragm will significantly increase the effective diameter. This could explain in part why the switching up pressure agrees with the switching down pressure for the larger diaphragms and diverges as the diaphragms get smaller. Additionally, the delamination might propagate with each successive switching. Many of these die were switched back and forth numerous times, not just the handful used for data collection.

Alternatively the boundary condition at the wall of the diaphragm and silicon substrate could be having an effect on the actuation pressure. Figure 41 is an image from die B. The edge of the diaphragm appears jagged.

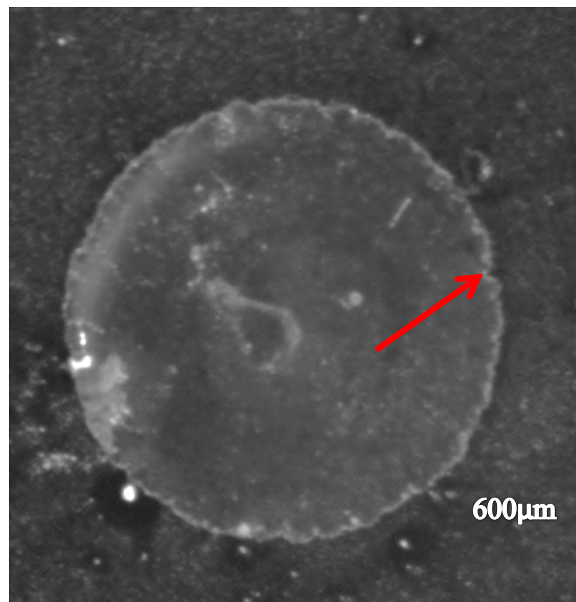

Figure 41. Image of diaphragm showing boundary conditions (highlighted).

The DRIE process leaves silicon "grass" or long micro-columns of silicon [17]. This results in a wall that is not completely uniform, like theory and ANSYS assume. The silicon "grass" similar to what the sidewalls of these diaphragms look like is shown in Figure 42.

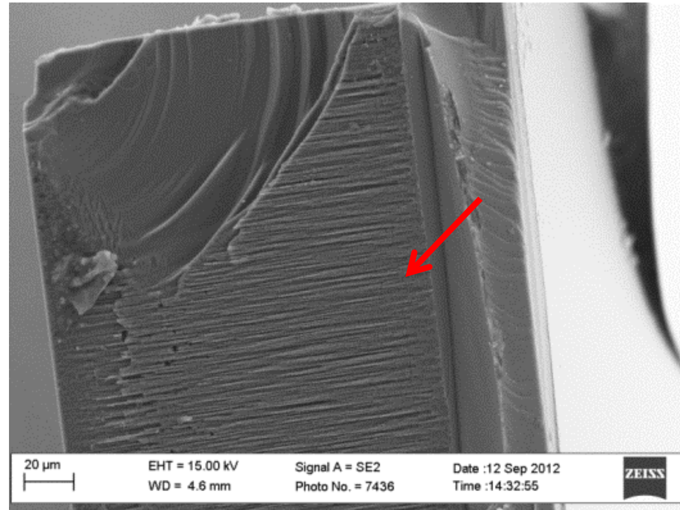

Figure 42. SEM image of a sidewall showing silicon "grass" (highlighted).

This “grass” effect leaves an irregular wall. The larger the area to be etched using DRIE the better the wall looks. Additionally these sidewall effects are less dominant in a larger diameter diaphragm structure. An image from a sectioned diaphragm is shown in Figure 43. The micro-columns shown in Figure 43 get larger as the depth increases. The wall at the bottom of the wafer appears smooth. Conversely, the top is quite coarse. The amount of coarseness and variations in the wall vary from diaphragm to diaphragm.

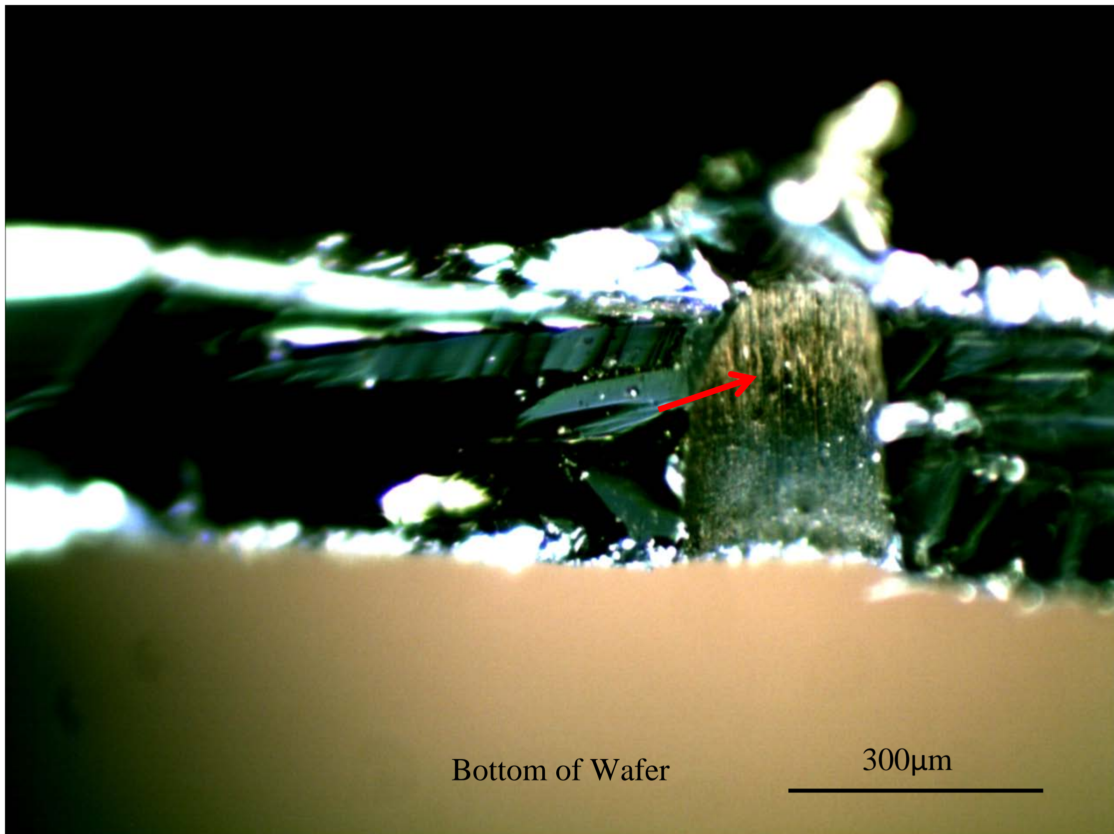

Figure 43. Diaphragm section showing silicon micro-columns or "grass". 300MPa compressive stress. Polyimide 3.8µm / SiO_2 0.4µm.

Another potential effect common to DRIE is undercutting, where the silicon at the bottom of the trench cuts under the feature. This is illustrated in Figure 44. Undercutting is not necessarily uniform and in conjunction with the “grass” effect could have a significant impact on the boundary conditions. The theoretical and ANSYS models assume a completely uniform, infinitely-stiff boundary. Some of these effects can be seen in a diaphragm that was not fully opened with the DRIE shown in Figure 45.

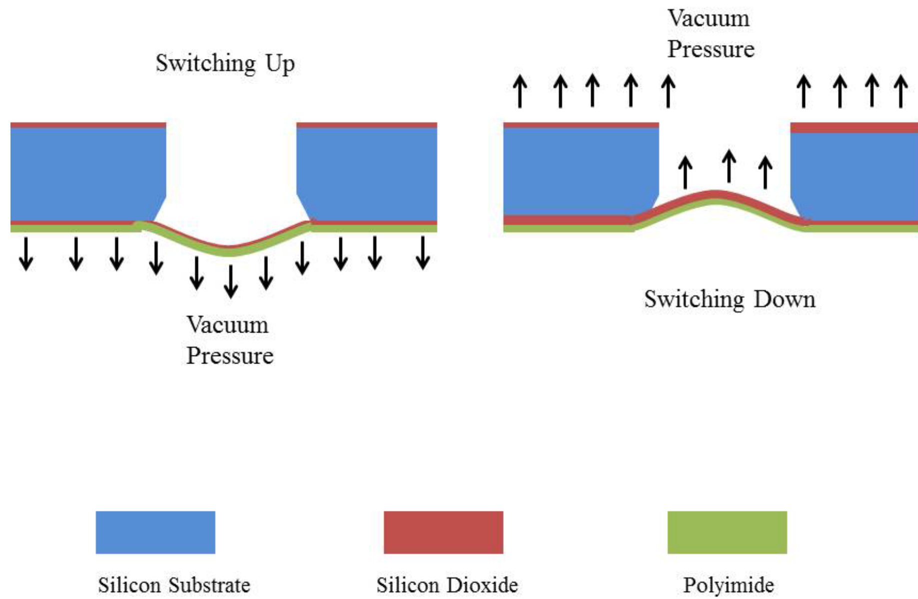

Figure 44. Illustration of undercutting and its effect on switching.

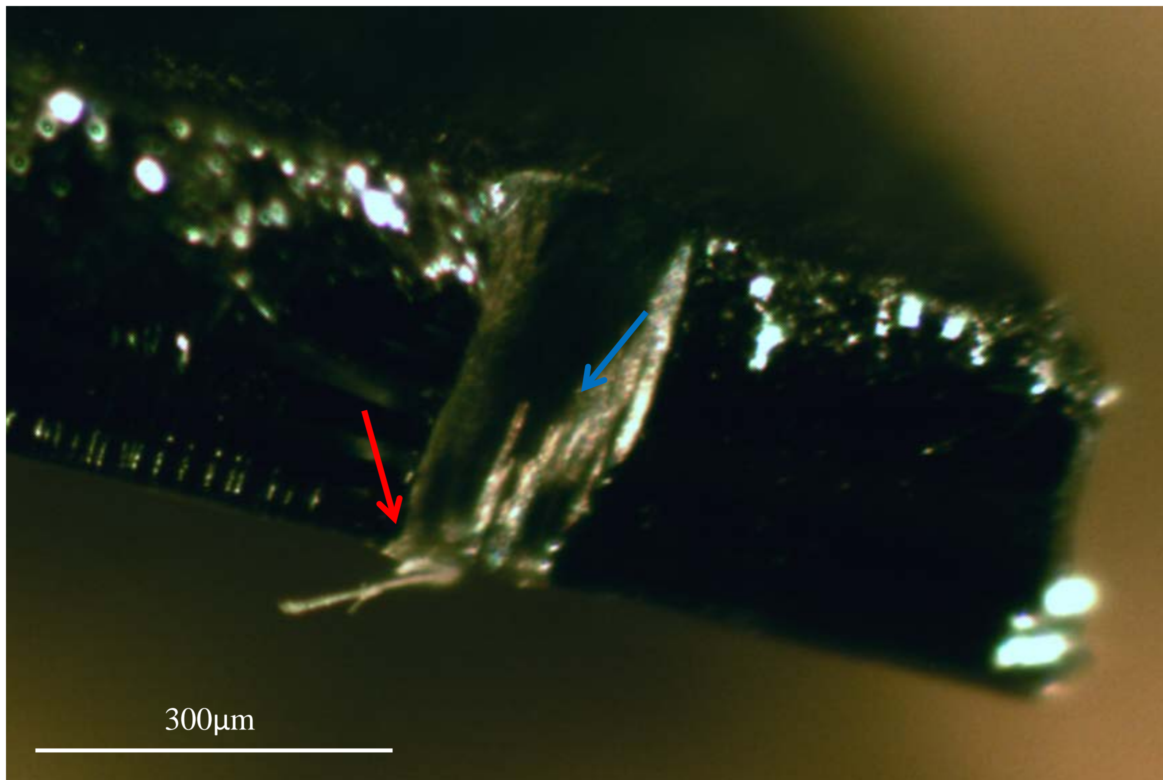

Figure 45. Cross-section of a diaphragm showing effects of DRIE (undercutting – red arrow, "grass" – blue arrow). 300MPa compressive stress. Polyimide 3.8µm / SiO_2 0.4µm.

The diaphragm shown in Figure 45 was not etched all the way through leaving silicon "grass" on the surface of the diaphragm. Since this diaphragm was not completely etched, the effects of the DRIE process are a little more pronounced. The silicon grass is usually confined to the edges and is not as large.

The opposite of undercutting is a radius at the end of the trench. This effect is shown in Figure 46 from Chen *et al*. who conducted extensive work on the variations in DRIE [17].

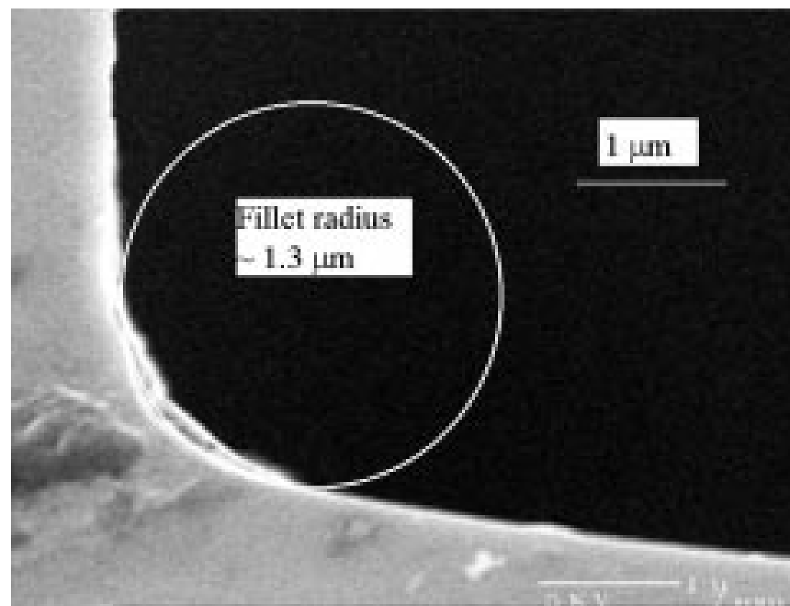

Figure 46. DRIE trench radius, Chen *et al*. [17].

The effect of this radius has a significant impact on the boundary condition. The bending moment in the diaphragm is no longer supported as a cantilever from theory, but is distributed into the silicon a little more. All of these possibilities are difficult to verify without sectioning each diaphragm with techniques such as focused ion beam milling.

Another possible explanation for the discrepancies between experimental results and model predictions is non-eigenvalue buckling. The two models assume eigenvalue buckling or axisymmetric buckling. Figure 47 shows the progression of a dimple forming on a diaphragm as it buckles down.

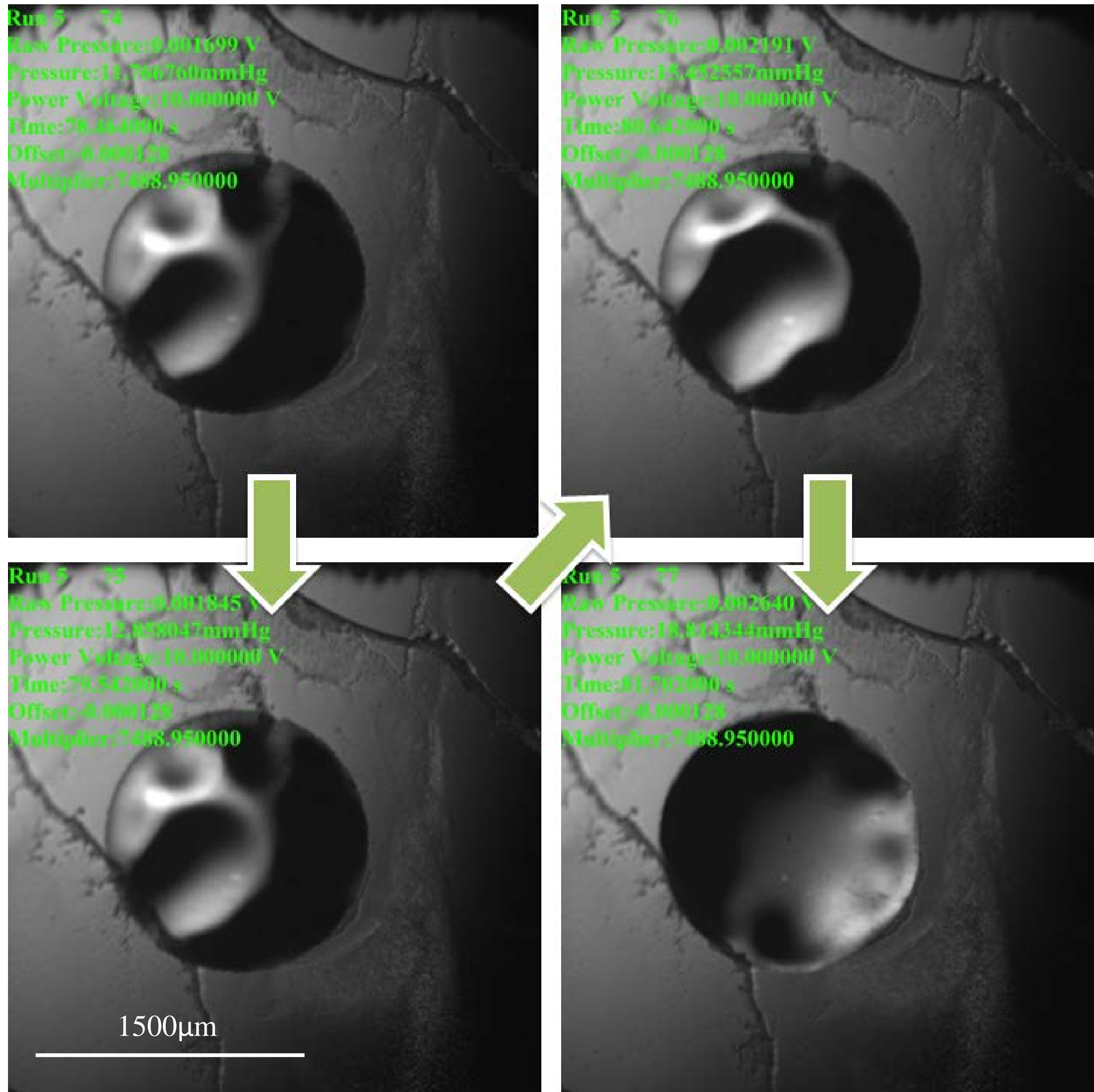

Figure 47. Die E, 1500µm diaphragm, non-eigenvalue buckling down. 300MPa compressive stress. Polyimide 3.8µm / SiO_2 0.4µm.

The progressive images in Figure 47 clearly show a dimple forming on the diaphragm and progressing across the diaphragm as a function of pressure. The diaphragm shown here is from die E with a diameter of 1.5mm or 1500µm. ANSYS predicted a larger switching pressure for die E than was experimentally determined, Figure 38. Due to the large size of the diaphragm and very large slenderness ratio, the dimple is more pronounced than on smaller diaphragms. The same behavior was witnessed for some of the diaphragms in the 900µm to 800µm range. However, due to the sampling rate of the data acquisition system, this behavior could not be captured as clearly as that in Figure 47. The dimple may form due to imperfections in the polyimide or silicone dioxide layers. The models assume completely uniform and homogenous layers. In practice, though, this is rarely the case.

Actuation pressure goes down as the diameter of a diaphragm increases. This is supported by both finite element modeling and experimental results. ANSYS consistently over-predicts the actuation pressure for experimentally switching up, which is likely due to boundary conditions created by DRIE or delamination. ANSYS models the experimentally switching down data well for the larger diameter membranes, between 400µm and 900µm. As the diaphragm diameter gets smaller, less than 300µm, the argument of the radical from equation (4) approaches zero. Current theoretical models do not predict buckling as the diameters continue to get smaller. The ANSYS data for these small diaphragms begins to drop off. Experimentally, the diaphragms lose their bi-stability behavior. There is not a significant difference in the actuation pressure data between the dies with distant diaphragms and the arrays with closely spaced diaphragms. Very large diameter diaphragms exhibit non-eigenvalue buckling and are poorly modeled

by the current finite element model. Buckled height data between ANSYS and experimental results agrees very closely, suggesting the boundary conditions do not significantly impact the buckled height.

V. CONCLUSIONS

Bi-stable buckled diaphragms were created in the clean room using information from previous work [14]. These devices were tested in a newly fabricated test fixture that utilized O-rings, a functional improvement over older test fixtures. A finite element model using Shell209 elements was created to model the pressure switching behavior of the diaphragms. The larger diaphragms, 350μm - 900μm diameter range, showed relatively good agreement with the finite element model. The buckled heights for all of the diaphragms matched very well with those predicted by the finite element model. The discrepancies between experimental and modeled behavior are likely due to boundary conditions or other micro-machining effects. Future work will involve the continued development of a more sophisticated finite element model and 3D DIC.

VI. FUTURE WORK

A different ANSYS model that better models the response of the smaller diaphragms in the range of 200μm - 350μm could be developed. This model could use a varying radius at the diaphragm-sidewall interface to better approximate the boundary conditions. A preliminary model has already been developed using Plane183 elements and Shell209 elements in an axisymmetric configuration about the y-axis, or left line. Plane183 elements extend into 10% of the diaphragm. Shell elements are useful for their limited number of degrees of freedom and are computationally less intensive. The more linear portions of the diaphragm can be modeled with shell elements without much loss in behavior. The element plot of model is shown in Figure 48; the teal elements are the shells and cover the majority of the diaphragm. The purple elements are the planes. A mapped mesh of the plane elements was used, with two elements and five elements through the thickness of the silicon dioxide and polyimide layers respectively. There are 20 shell elements along the length and 10 elements along the length of the plane portion of the diaphragm. Finally, there are 15 elements along the length of the wall plane elements. The wall plane elements are constrained not move vertically, the far right line is fixed in all degrees of freedom. An eigenvalue buckling analysis of this model has already been done and is illustrated in Figure 49.The first mode of buckling is shown in figure. The shell elements appear to be disconnected from the Plane183 elements, but this is not the case, just an artifact of element shape expansion.

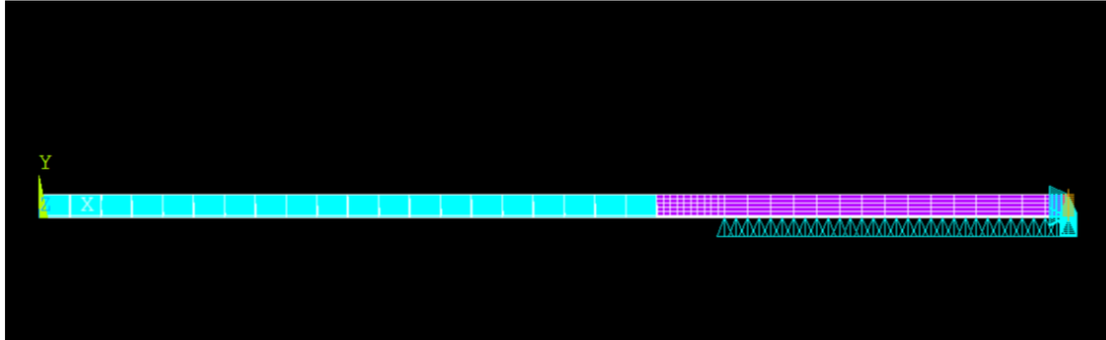

Figure 48. Element plot in ANSYS of new model showing element type (shells - teal, plane - purple) and boundary conditions.

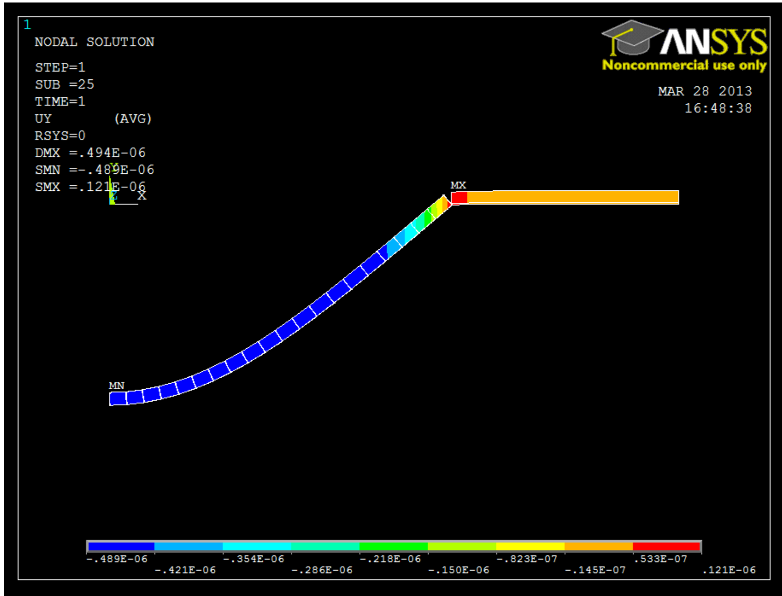

Figure 49. Eigenvalue buckling analysis showing shell and plane elements.

Three dimensional DIC or direct image correlation could be done to calculate the stresses in the diaphragm. This method would be very beneficial for the non-eigenvalue buckling cases. 1750μm and 1500μm diaphragms from die E have already been speckled for use in 3D DIC. An image from die E is shown in Figure 50. The black spots form a unique pattern on the surface of the diaphragm. With the use of a stereoscope and

independent optical paths, 3D DIC can be performed. The relative displacements of the black spots are calculated from the pixel information in a computer program. This displacement is directly related to the strain in the film using standard mechanics of materials equations.

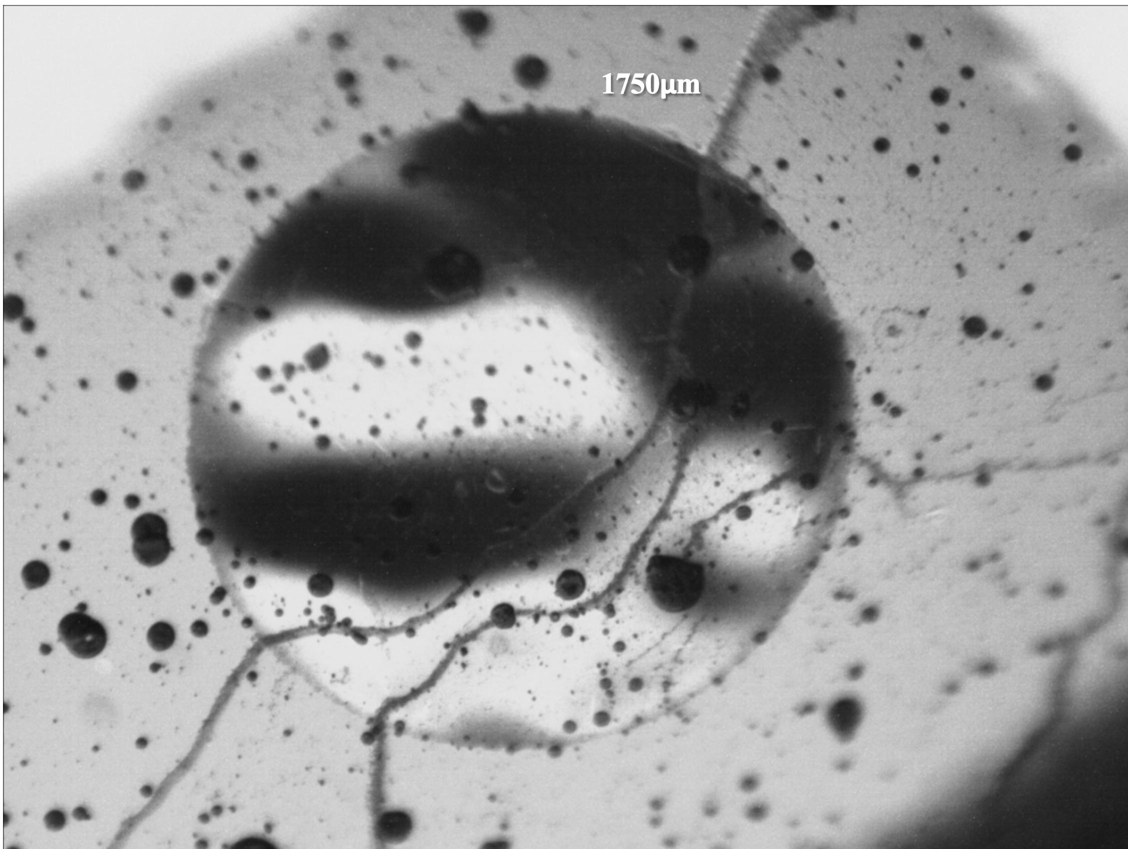

Figure 50. Speckled image from die E. 300MPa compressive stress. Polyimide 3.8μm / SiO_2 0.4μm.

VII. REFERENCES

[1] Asadnia, Kottapalli, Shen, Miao, Barbastathis, Triantafyllou, "Flexible, zero powered, piezoelectric MEMS pressure sensor arrays for fish-like passive underwater sensing in marine vehicles," *Micro Electro Mechanical Systems (MEMS), 2013 IEEE 26th International Conference on* , vol., no., pp.126,129, 20-24 Jan. 2013

[2] Arya, Rashid, Collins, Smith. "Thermally Actuated, Bi-Stable, Snapping Silicon Membranes", *Transducers '03, 12th International Conference on Solid State Sensors, Acutaors and Microsystems*, pp.1411-1414. 2003

[3] Glos, Sauser, Papautsky, Bylski-Austrow, "Implantable MEMS compressive stress sensors: Design, fabrication and calibration with application to the disc annulus". *Journal of Biomechanics*. 2010.

[4] Holmes, Gates, Smith, "Integrated optical differential pressure transducers achieved using thin buckled silica membranes and direct UV written planar Bragg gratings", *Sensors and Actuators A: Physical*. 2011

[5] Jozwik, Delobelle, Gorecki *et al.,* "Optomechanical characterization of compressively prestressed silicon oxynitride films deposited by plasma-enhanced chemical vapour deposition on silicon membranes". *Thin Solid Films 468*, pp.84-92. 2004.

[6] Prochazka, Meier, Viggiani, Roesgen, "Optically interrogated MEMS pressure sensor array" *Exp Fluids.* Vol.52, pp1003-1015, 2012.

[7] Timoshenko, Woinowsky-Krieger. 1959. *Theory of Plates and Shells.* 2nd. Ed. McGraw-Hill Book Company, New York.

[8] Gowrishetty, Usha. 2010-12. Unpublished Work on bi-stable buckled diaphragms. J.B. Speed School of Engineering, University of Louisville.

[9] Reck, Thomsen, and Hansen "All-Optical Frequency Modulated High Pressure MEMS Sensor for Remote and Distributed Sensing". *Sensors* 2011.

[10] Schomburg and Goll, "Design optimization of bistable microdiaphragm valves". *Sensors Actuators A*. Vol. 64 pp259-264. 1997.

[11] Porter, Gowrishetty, Phelps, Walsh, Berfield. "Mechanics of Buckled Structure MEMS for Actuation and Energy Harvesting Applications" *ASME IMECE 2012 Proceedings*. 2012.

[12] Ziebart, Paul and Baltes. "Strongly Buckled Square Micromachined Diaphragms" *Journal of Microelectromechanical Systems*. Vol. 8, No. 4, December 1999.

[13] Ayela and Nicu *et al*. "Determination of d31 piezoelectric coefficient of the PbZrxTi1-xO3 thin films using multilayer buckled microdiaphragms", *Journal of Applied Physics* 100. 2006.

[14] Gowrishetty, Walsh, Berfield. "Fabrication of polyimide bi-stable diaphragms using oxide compressive stresses for the field of 'Buckle MEMS'" *Journal of Micromechanics Microengineering* vol.20. 2010.

[15] G.G. Stoney,"The Tension of Metallic Films Deposited by Electrolysis", *Proceedings of the Royal Society of London A,* Vol.82 pp. 172-175, 1909.

[16] Ozsun, Alaca, Yalcinkaya *et al*., "On heat transfer at microscale with implications for microactuator design", *Journal of Micromechanics Microengineering* Vol.19. 2009.

[17] Chen and Ayon "Effect of Process Parameters on the Surface Morphology and Mechanical Performance of the Silcon Structures After Deep Reactive Ion Etching (DRIE)". *Journal of Microelectromechanical systems*. Vol. 11, No. 3. 2002

VIII. APPENDIX I

ANSYS Simulation Buckling Down Input File

```
FINISH
/CLEAR,NOSTART

/PREP7

! Diaphragm Diameter in meters
Diameter=400e-6                    !Change value for each diaphragm size

! SiO2 Thicknesss (meters)
SiO2thk=.4e-6

! Polyimide Thickness (meters)
Polythk=3.8e-6

Subsets1=1000
AppPress1=28500
DeltaP=1000
Subsets2=2000
AppPress2=AppPress1+DeltaP

!Applied Temperature and CTE
            ! T = 822 old, T= 851.2 New
AppTemp = 851.2
CTE = 4e-6

ET,1,SHELL209
KEYOPT,1,8,2
KEYOPT,1,9,0
!KEYOPT,1,10,1

!Properties and shell sections----------------
MPTEMP,,,,,,,,
MPTEMP,1,0
MPDATA,EX,1,,73e9
MPDATA,PRXY,1,,.17
MPTEMP,,,,,,,,
MPTEMP,1,0
UIMP,1,REFT,,,
MPDATA,ALPX,1,,CTE

MPTEMP,,,,,,,,
MPTEMP,1,0
MPDATA,EX,2,,8e9
MPDATA,PRXY,2,,.2
MPTEMP,,,,,,,,
MPTEMP,1,0
UIMP,2,REFT,,,
MPDATA,ALPX,2,,0            !3.3124e-6

sect,1,shell,,Membrane
secdata, SiO2thk,1,0.0,3
secdata, Polythk,2,0.0,3
secoffset,MID
seccontrol,,,, , , ,

!Create keypoints and lines-----------------
KEYOPT,1,8,2
```

```
KEYOPT,1,9,0
!KEYOPT,1,10,1

K, ,0,0,,
K, ,Diameter/2,0,,
LSTR,       1,       2

!Mesh Line----------------------------------
FLST,5,1,4,ORDE,1
FITEM,5,1
CM,_Y,LINE
LSEL, , , ,P51X
CM,_Y1,LINE
CMSEL,,_Y

LESIZE,_Y1, , ,100, , , , ,1

CM,_Y,LINE
LSEL, , , ,       1
CM,_Y1,LINE
CMSEL,S,_Y

LMESH,       1



!Set up Load Steps 1 through 5----------------------

!Load Step 1------------------------
FLST,2,1,3,ORDE,1
FITEM,2,2

DK,P51X, ,0, ,0,ALL, , , , , ,
FLST,2,1,4,ORDE,1
FITEM,2,1

SFL,P51X,PRES,-1000,
FINISH
/SOL
ANTYPE,0
NLGEOM,1
NSUBST,10,10,10
OUTRES,ERASE
OUTRES,ALL,1
TIME,.001
LSWRITE,1,



!Load Step 2----------------
FLST,2,1,4,ORDE,1
FITEM,2,1

BFL,P51X,TEMP,AppTemp
NSUBST,100,100,100
TIME,.002
LSWRITE,2,



!Load Step 3---------------------
FLST,2,1,3,ORDE,1
```

```
FITEM,2,2

DK,P51X, ,0, ,0,ALL, , , , , ,
FLST,2,1,4,ORDE,1
FITEM,2,1

SFL,P51X,PRES,0,

NSUBST,10,10,10
TIME,.003
LSWRITE,3,


!Load Step 4--------------------
FLST,2,1,4,ORDE,1
FITEM,2,1

SFL,P51X,PRES,AppPress1,
NSUBST,Subsets1,Subsets1,Subsets1
TIME,abs(AppPress1)
LNSRCH,1
NEQIT,5000
STABILIZE,CONSTANT,ENERGY,.5e-4,NO
LSWRITE,4,

!Load Step 5--------------------
FLST,2,1,4,ORDE,1
FITEM,2,1

SFL,P51X,PRES,AppPress2,
NSUBST,Subsets2,Subsets2,Subsets2
TIME,abs(AppPress2)
LNSRCH,1
NEQIT,5000
STABILIZE,CONSTANT,ENERGY,.5e-4,NO
LSWRITE,5,



!Load Step 6---------------------
FLST,2,1,4,ORDE,1
FITEM,2,1
/GO

SFL,P51X,PRES,0,

NSUBST,40,40,40
TIME,abs(AppPress1)+1
LSWRITE,6,

!SOLVE--------------------
LSSOLVE,1,6,1,

!THPP----------------------------
FINISH
/POST26
FILE,'Shell','rst','.'
/UI,COLL,1
NUMVAR,200
SOLU,191,NCMIT
STORE,MERGE
```

```
FILLDATA,191,,,,1,1
REALVAR,191,191

NSOL,2,1,U,Y, UY_2
STORE,MERGE
FORCE,TOTAL
SHELL,TOP


ESOL,3,1,1 ,SMISC,14,Pressure
STORE,MERGE
XVAR,2
PLVAR,3,

!NUMVAR,200
FILLDATA,191,,,,1,1
REALVAR,191,191
PRVAR,2,3,
```

IX. APPENDIX II

ANSYS Buckling Up Input File

```
FINISH
/CLEAR,NOSTART

/PREP7

!Diaphragm Diameter in meters
Diameter=600e-6                 !Change for each diaphragm size

! SiO2 Thicknesss (meters)
SiO2thk=.4e-6

! Polyimide Thickness (meters)
Polythk=3.8e-6

Subsets1=500
AppPress1=-2000
DeltaP=1000
Subsets2=Subsets1
AppPress2=AppPress1-DeltaP

!Applied Temperature and CTE
          ! T = 822 old, T= 851.2 New
AppTemp = 851.2
CTE = 4e-6

ET,1,SHELL209

KEYOPT,1,8,2
KEYOPT,1,9,0
!KEYOPT,1,10,1

!Properties and shell sections----------------
!SiO2
MPTEMP,,,,,,,,
MPTEMP,1,0
MPDATA,EX,1,,73e9
MPDATA,PRXY,1,,.17
MPTEMP,,,,,,,,
MPTEMP,1,0
UIMP,1,REFT,,,
MPDATA,ALPX,1,,CTE

!Polyimide
MPTEMP,,,,,,,,
MPTEMP,1,0
MPDATA,EX,2,,8e9
MPDATA,PRXY,2,,.2
MPTEMP,,,,,,,,
MPTEMP,1,0
UIMP,2,REFT,,,
MPDATA,ALPX,2,,0          !3.3124e-6

sect,1,shell,,Membrane
secdata, SiO2thk,1,0.0,3
secdata, Polythk,2,0.0,3
secoffset,MID
seccontrol,,,, , , ,
```

```
!Create keypoints and lines-----------------
KEYOPT,1,8,2
KEYOPT,1,9,0
!KEYOPT,1,10,1


K, ,0,0,,
K, ,Diameter/2,0,,
LSTR,       1,       2

!Mesh Line----------------------------------
FLST,5,1,4,ORDE,1
FITEM,5,1
CM,_Y,LINE
LSEL, , , ,P51X
CM,_Y1,LINE
CMSEL,,_Y

LESIZE,_Y1, , ,100, , , , ,1

CM,_Y,LINE
LSEL, , , ,       1
CM,_Y1,LINE
CMSEL,S,_Y

LMESH,       1



!Set up Load Steps 1 through 5----------------------

!Load Step 1------------------------
FLST,2,1,3,ORDE,1
FITEM,2,2


DK,P51X, ,0, ,0,ALL, , , , , ,
FLST,2,1,4,ORDE,1
FITEM,2,1


SFL,P51X,PRES,1000,
FINISH
/SOL
ANTYPE,0
NLGEOM,1
NSUBST,10,10,10
OUTRES,ERASE
OUTRES,ALL,1
TIME,.001
LSWRITE,1,



!Load Step 2----------------
FLST,2,1,4,ORDE,1
FITEM,2,1

BFL,P51X,TEMP,AppTemp
NSUBST,100,100,100
TIME,.002
```

```
LSWRITE,2,

!Load Step 3---------------------
FLST,2,1,3,ORDE,1
FITEM,2,2

 DK,P51X, ,0, ,0,ALL, , , , , ,
FLST,2,1,4,ORDE,1
FITEM,2,1

SFL,P51X,PRES,0,

NSUBST,10,10,10
TIME,.003
LSWRITE,3,

!Load Step 4--------------------
FLST,2,1,4,ORDE,1
FITEM,2,1

SFL,P51X,PRES,AppPress1,
NSUBST,Subsets1,Subsets1,Subsets1
TIME,abs(AppPress1)
LNSRCH,1
NEQIT,5000
STABILIZE,CONSTANT,ENERGY,.5e-4,NO
LSWRITE,4,

!new
!Load Step 5--------------------
FLST,2,1,4,ORDE,1
FITEM,2,1

SFL,P51X,PRES,AppPress2,
NSUBST,Subsets2,Subsets2,Subsets2
TIME,abs(AppPress2)
LNSRCH,1
NEQIT,5000
STABILIZE,CONSTANT,ENERGY,.5e-4,NO
LSWRITE,5,

!Load Step 6---------------------
FLST,2,1,4,ORDE,1
FITEM,2,1

SFL,P51X,PRES,0,

NSUBST,40,40,40
TIME,abs(AppPress1)+1
LSWRITE,6,

!SOLVE--------------------
LSSOLVE,1,6,1,

!THPP----------------------------
FINISH
/POST26
FILE,'Shell','rst','.'
/UI,COLL,1
NUMVAR,200
SOLU,191,NCMIT
STORE,MERGE
```

```
FILLDATA,191,,,,1,1
REALVAR,191,191

NSOL,2,1,U,Y, UY_2
STORE,MERGE
FORCE,TOTAL
SHELL,TOP


ESOL,3,1,1 ,SMISC,14,Pressure
STORE,MERGE
XVAR,2
PLVAR,3,

!NUMVAR,200
FILLDATA,191,,,,1,1
REALVAR,191,191
PRVAR,2,3,
```